[American Journal of Science, Vol. 302, September, 2002, P. 549–581]

American Journal of Science

SEPTEMBER 2002

PROLONGED ACADIAN OROGENESIS: REVELATIONS FROM FOLIATION INTERSECTION AXIS (FIA) CONTROLLED MONAZITE DATING OF FOLIATIONS IN PORPHYROBLASTS AND MATRIX

T. H. BELL and P. W. WELCH

School of Earth Sciences, James Cook University,
Townsville, Queensland 4811, Australia

ABSTRACT. Numerous phases of garnet growth are revealed by detailed studies of foliation inflection/intersection axes preserved in porphyroblasts (FIAs) in Acadian metamorphic rocks in the Chester Dome region of Vermont, in the United States of America. A regionally consistent succession of four different FIA trends in garnet porphyroblasts has been dated by analyzing monazite inclusions with an electron microprobe. These monazite inclusions, which lie within the various foliations that define the FIAs, provide absolute ages for multiple periods of deformation and episodic phases of garnet growth. The monazite inclusions reveal a progression in foliation ages from 431±2 to 349±3 million years within porphyroblasts and from 366±3 to 327±5 million years in pervasive matrix foliations. Three samples of schist reveal ages ranging through 75 to 70 million years from the cores of porphyroblasts, through the medians to the rims and then into the matrix. Ages determined from monazite grains within garnet porphyroblasts link directly to periods of multiple deformation and episodic garnet growth defined by the FIAs. The four FIA sets began forming prior to 424±3, 405±6, 386±6 and 366±4 million years ago, respectively. Thus multiple stages of garnet growth occurred throughout Acadian deformation and metamorphism in Vermont, and orogenesis was far more prolonged than previously thought. Invariably, garnet growth occurred early in the accompanying deformation event.

Dating of monazite inclusions without careful separation of phases of garnet growth by FIA studies will lead to a spread of ages that will confuse rather than elucidate the metamorphic and structural history. Analysis of monazite grains in the matrix alone will likely only present ages for the youngest events. These ages can be amalgamated from grain to grain to yield apparently precise ages, but such ages reveal nothing about the deformation and metamorphic processes operating during orogenesis, or the overall continuity of the deformation and metamorphism that accompanies plate motion. FIA and microstructural studies of inclusion trail successions allow numerous phases of garnet growth to be distinguished and then dated using monazite that has dissolved and regrown many times as multiple successive foliations developed. This in turn allows very long and involved metamorphic histories to be fully integrated with similarly complex structural histories.

INTRODUCTION

The rocks around the Chester and Athens Domes (fig. 1) have been the basis for a significant amount of fundamental metamorphic petrological work from the fifties through to the nineties by Thompson (1957), Thompson and Thompson (1976), Thompson and others (1977) and Vance and Holland (1993). They also provided the source for the garnets containing spiral inclusion trail studies by Rosenfeld (1968, 1970). They are a remarkable group of rocks because inclusion trails and compositional zoning in porphyroblasts are preserved in almost every sample, potentially allowing the metamorphic and structural history to be fully integrated. Extremely detailed microstructural studies of these rocks began in 1985 and, more recently, we

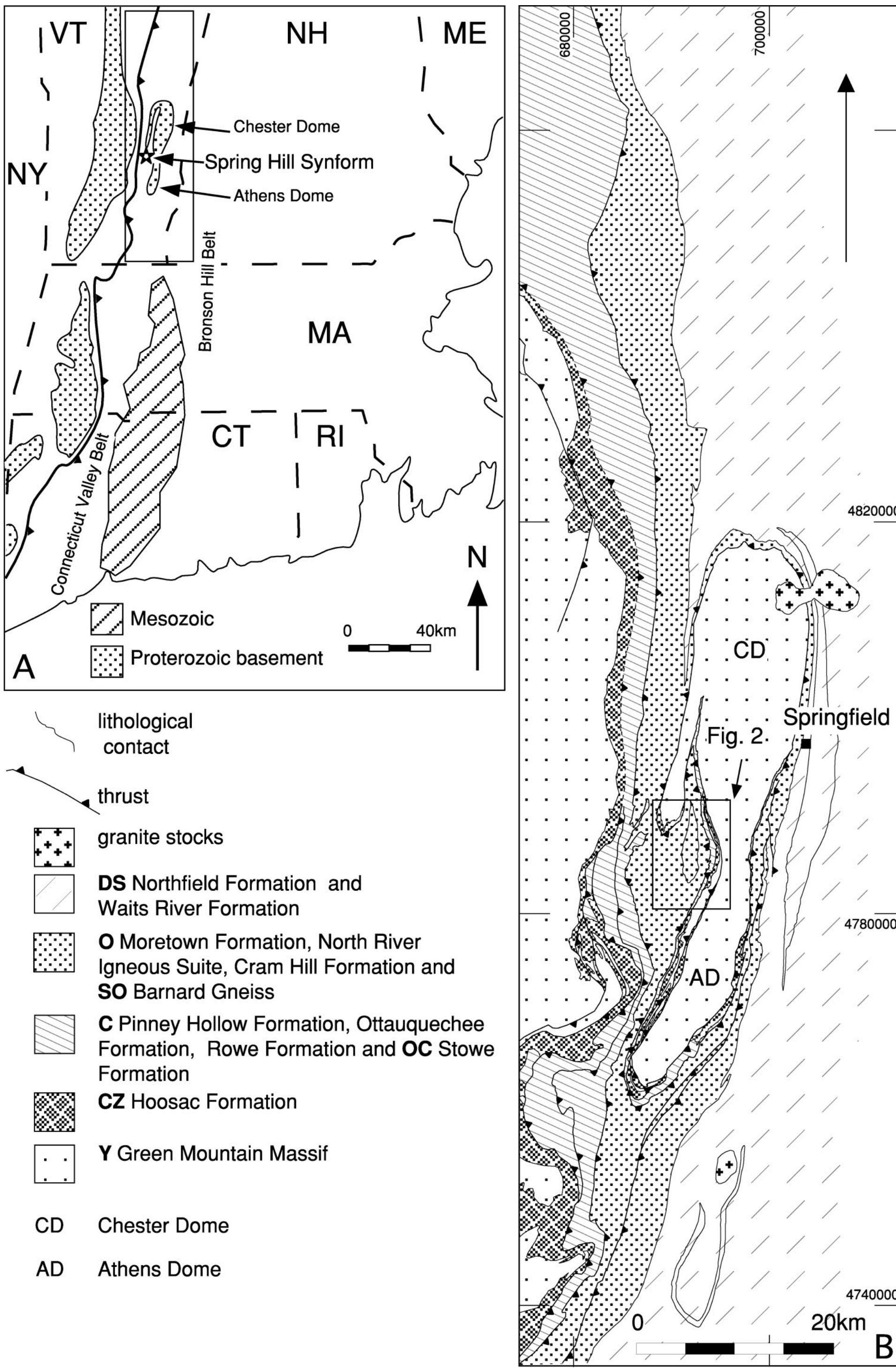

Fig. 1. (A) Location of the region around the Chester and Athens domes (marked by rectangular box). (B) Geological map of the region around the Chester and Athens domes in SE Vermont. Geology after Doll *et al.* (1961); Ern (1963); Hepburn *et al.*, (1984); Stanley and Ratcliffe, 1985; Thompson *et al.* (1990); Ratcliffe *et al.* (1992); Ratcliffe (1993, 1995a, b); Ratcliffe and Armstrong (1995, 1996).

have been attempting to integrate those studies with similarly detailed metamorphic studies using the controls on timing and separation of periods of metamorphic growth provided by the microstructural work.

Structural (Hickey and Bell, 2001) and microstructural work (Bell and Hickey, 1997; Bell and others, 1998; Ham, ms, 2001) using newly developed quantitative methods has revealed a more extensive history of deformation and metamorphism than previously recognized for any rocks in the earth's crust. These methods have resulted in the recognition of successions of multiple porphyroblast growth and foliation development and provided a powerful means for establishing relative timing. This in turn has supplied a way of dating multiple metamorphic events using monazite grains that grew, dissolved or recrystallized and regrew as successive foliations developed. Monazite grains later overgrown by garnet porphyroblasts, are preserved and shielded from subsequent dissolution and regrowth occurring within the matrix foliation that preserves only the very latest deformational history.

This paper reports the results of dating monazite preserved as inclusions in successive foliations moving outwards from the core to rim of garnet porphyroblasts. These foliations have been grouped into periods of foliation development and metamorphism by measurement of foliation inflection/intersection axes preserved as inclusion trails in porphyroblasts (FIAs). These FIAs have allowed the distinction of a succession of four periods of metamorphism and foliation development in the region around the Chester and Athens domes (Bell and others, 1998) over an area greater than 4000 square kilometers. The successful microprobe dating of monazite grains associated with multiple foliations outwards from the core for successive FIA sets has revealed a consistent and extensive deformation and metamorphic history for southeast Vermont.

GEOLOGICAL SETTING

Middle Proterozoic basement gneisses of the Chester and Athens Domes are unconformably overlain by the Late Proterozoic to Early Cambrian Hoosac Formation (Stanley and Ratcliffe, 1985; Ratcliffe and others, 1992). These rocks were overthrust by a eugeoclinal sequence of Cambrian to Middle Ordovician calcareous, pelitic and semi-pelitic metasedimentary and, mainly mafic, metavolcanic and intrusive rocks of the Rowe-Moretown (or Rowe-Hawley) lithotectonic unit (fig. 1). The youngest lithotectonic unit in southeast Vermont is the thick Siluro-Devonian sequence of the Connecticut Valley Trough, separated from the Cambro-Ordovician rocks to the west by an angular unconformity (Ratcliffe, 1993, 1995a, 1995b; Ratcliffe and Armstrong, 1995).

In southeastern Vermont two distinct periods of deformation and metamorphism have been recognized as the Ordovician Taconic and Devonian Acadian orogenies (Stanley and Ratcliffe, 1985; Armstrong and others, 1992). Taconian metamorphism predominates to the west of the Green Mountain Massif while the affects of the Acadian orogeny predominate to the east. Spear and Harrison (1989) documented $^{40}Ar/^{39}Ar$ ages as old as 440 Ma to the east of the Green Mountain Massif and have interpreted these to be partially reset Taconian ages. The Acadian Orogeny involved the closure of the Siluro-Devonian basin comprising the Connecticut Valley Trough. This orogeny caused extensive folding of the entire Proterozoic to Devonian sequence (Bradley, 1983; Hepburn and others, 1984; Armstrong and others, 1992; Ratcliffe and others, 1992; Ratcliffe, 1995a, 1995b; Ratcliffe and Armstrong, 1995). Acadian metamorphism in southeast Vermont peaked at about 730°C and 10.5 kb at 395-385 Ma, and, unlike parts of the orogen farther east, was apparently a consequence solely of crustal thickening with little or no magmatic heating (Armstrong and others, 1992; Ratcliffe and others, 1992; Vance and Holland, 1993).

All microstructural work on FIAs done to date shows the same progression of garnet growth in the Siluro-Devonian sequence as in the older units, indicating that mineral growth occurred during the Acadian Orogeny (Bell and others, 1998; Ham, ms, 2001). No folds or foliations of clear Taconic age have been identified in these studies although some are old enough to possibly lie in the transition from Taconic to Acadian. The FIAs and dates described herein come from the 35 x 125 km area extending from just north of the Massachusetts border in the south to some 50 kilometers north of the Chester Dome (fig. 1). Samples of metasedimentary, garnet bearing, non-carbonaceous quartz-mica schists and carbonaceous pelitic and semi-pelitic phyllites and schists were taken from a range of Cambrian (or late Proterozoic?) to Silurian stratigraphic units, mainly the Moretown, Northfield, Cram Hill and Waits River Formations (fig. 1). Samples selected for monazite dating were taken from pelitic to quartzose units of the Cram Hill formation. A sub-vertical N-S to NNE-SSW striking crenulation cleavage has formed as an axial plane structure to the domes. We call this cleavage S_5 after Hayward (ms, 1991; 1992). S_5 overprints a microscopically and mesoscopically prominent crenulation cleavage, S_4, that transects the axial plane to the Spring Hill synform lying to the west of the waist-like shape between the domes (fig. 2; Hickey and Bell, 2001). Microscopically, in areas of weaker S_5 development, S_4 has a sub-horizontal attitude and varies in intensity from open crenulations to a fully differentiated foliation that is axial planar to rootless folds in bedding and crenulations of an earlier foliation S_3 (Hickey and Bell, 2001). Therefore, it appears that folding during D_5 has rotated an originally sub-horizontal D_4. A sporadically developed sub-horizontal coarsely spaced crenulation, S_6, locally overprints S_5 (Hickey and Bell, 2001). No mesoscopic deformation fabrics earlier than S_3 were observed. Hayward (1992) argued that at least two additional foliations, which he called S_1 and S_2, are preserved in the porphyroblasts and we agree with this. Most large tight folds, like the Spring Hill Synform (fig. 2), appear to be pre-D_5 (Hickey and Bell, 2001). Some are D_4 structures, but others may be D_3 or earlier. Hayward (ms, 1991) found the asymmetry of S_4 on S_5 switched on either side of the Chester Dome, suggesting the latter is a D_5 feature. However, more recent work by Ham (ms, 2001) suggests the domes may be much older structures that were intensified during younger deformations.

SAMPLES DATED

The succession of FIA development in these rocks has been previously described by Bell and others (1998). In summary, across a 35 by 125 kilometer area, the rocks preserve a consistent succession of four FIA sets within garnet porphyroblasts trending successively SW-NE, W-E, NNW-SSE and SSW-NNE (fig. 3). The succession was determined using samples that preserve changes in FIA trend from core to rim or core to median to rim (Bell and others, 1998).

FIA set 1, as shown on the rose diagram in figure 4 of all FIAs measured from this region, lies on the edge of the distribution of FIA set 4. However, it is a distinct population (see small rose diagram inset on figure 4; a detailed statistical analysis is provided in Bell and others, 1998), as, with only one exception, it occurs only within the cores of porphyroblasts, with one of the other FIA sets preserved in the median or rim. In the one example where this is not the case, the inclusion trails are truncated by the matrix foliation in every vertical thin section cut around the compass used to measure the FIA (6 thin sections 30° apart with 2 more 10° apart close to the FIA). Where the inclusion trails define FIA set 4, they are always continuous with the matrix foliation in all or most thin sections cut around the compass (Bell and others, 1998).

Bell and others (1998) consider this succession of FIAs to reflect progressive changes in the direction of bulk shortening during Acadian orogenesis associated with changes in the direction of relative plate motion. They did not attempt to correlate foliations. Deformation is always heterogeneously distributed in the earth's crust and foliations can form from location to location at different times, and, in some locations, several foliations are preserved around individual FIAs. Rather, they argue that the

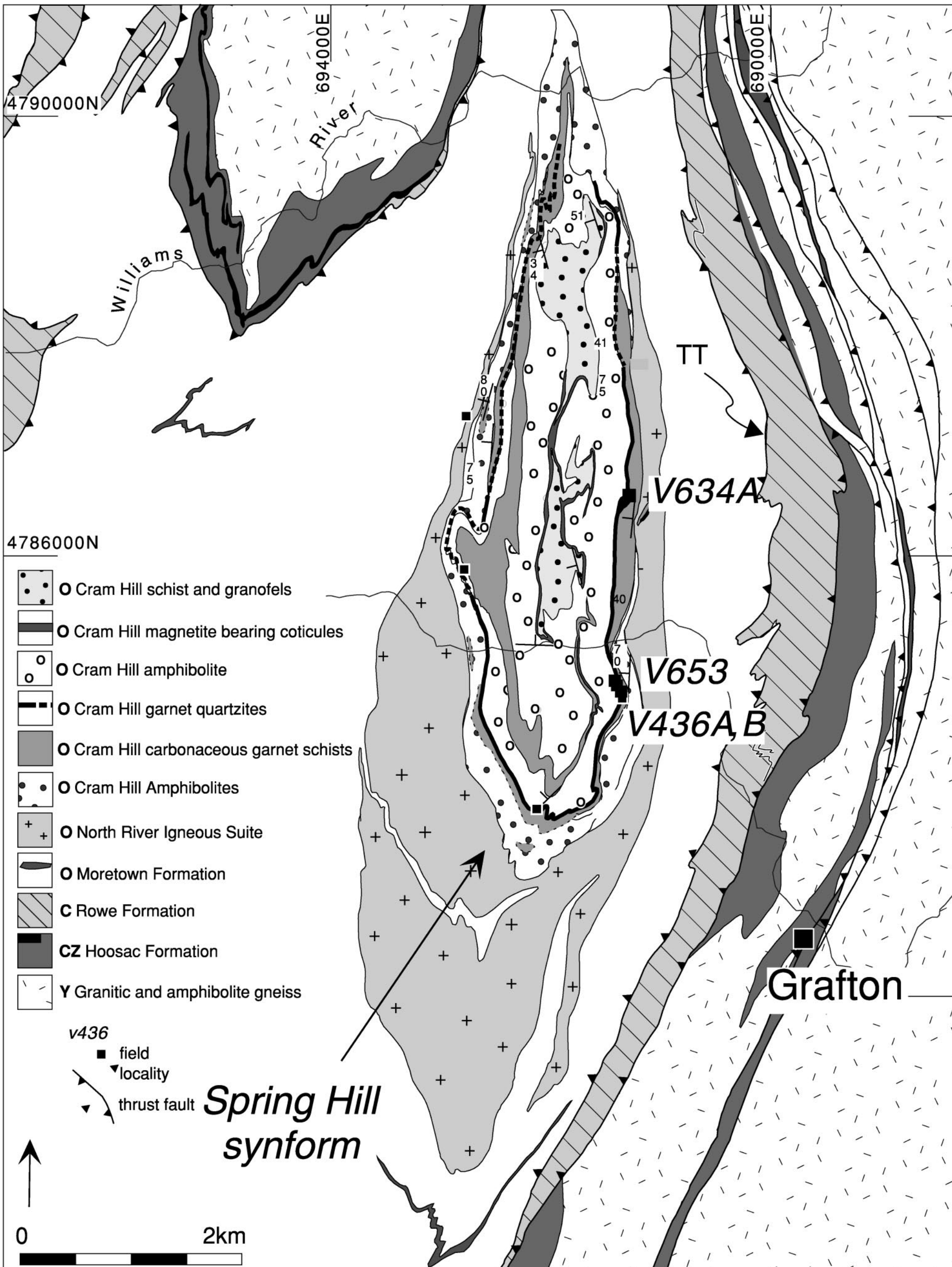

Fig. 2. Geological Map of the Spring Hill Synform showing the location of the samples dated. The location of this figure within the region around the Chester and Athens domes is shown in figure 1B. Main lithological relationships and structural features are those of Ratcliffe and Armstrong (1995, 1996) with some modification based on our own mapping in the area. TT = Townshend thrust.

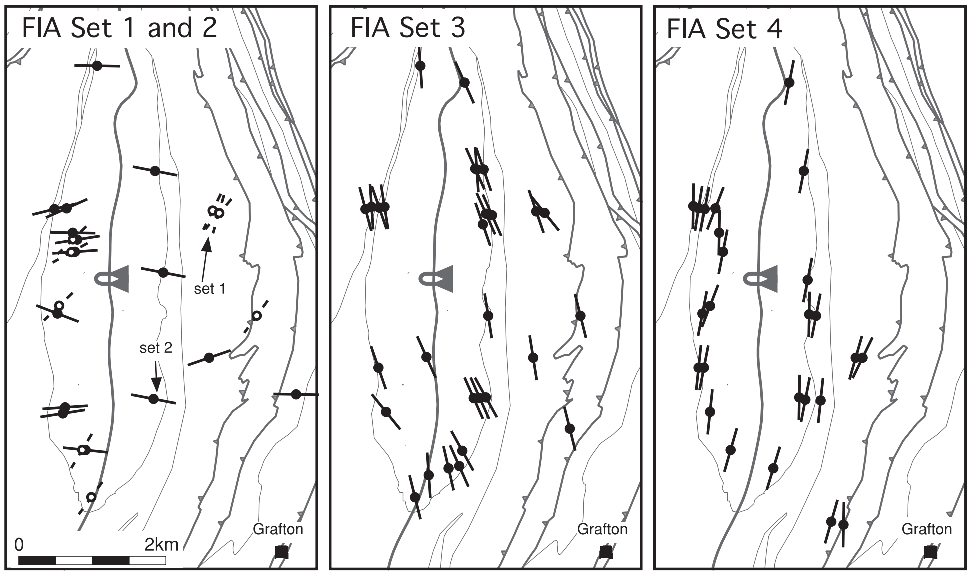

Fig. 3. Outline map of bedding across the Spring Hill synform showing the trends of successive FIA sets on each limb (modified from Bell and Hickey, 1997).

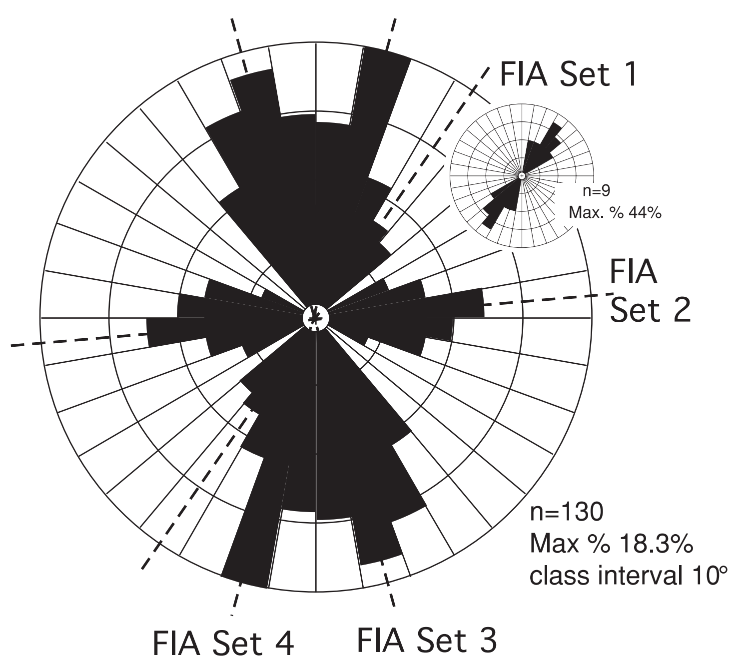

Fig. 4. Rose diagram showing the succession of four FIA sets within garnet porphyroblasts determined within the region around the Chester and Athens domes by Bell et al. (1998). The FIA sets trend successively SW-NE, W-E, NNW-SSE and SSW-NNE as shown. The SW-NE FIA set occurs on the edge of the large SSW-NNE set and is obscured by it because few samples preserve it. It is shown as an inset. See text for how it was separated from Set 4.

consistent succession of FIAs from sample to sample reflects periods of time over which the plate motion was constantly directed before shifting to another trend. This is supported by FIA data from the Alps where the relative plate motions that accompanied orogenesis are known (Bell and others, 1995).

Approximately 30 samples were examined to find monazite grains linked to the microstructures within the porphyroblasts. After inspection of the 8 or more thin sections cut per sample to determine the FIAs, at least two spatially oriented polished thin sections were prepared for each sample from the same blocks of rock used for the FIA determinations. Less than one third of these samples were found to contain monazite grains, with only half of those having sufficient monazite grains within porphyroblasts to make dating worth while. Samples with core - rim FIA relationships were chosen to test whether the monazite ages are consistent with the FIA succession determined microstructurally by Bell and others (1998). Only one sample containing the earliest FIA was found to have monazite present as inclusions; however, garnet growth in this sample occurred during development of the second FIA set. The succession and orientations of FIAs in the samples dated are shown in figures 3 and 4.

The four samples dated were taken from the Cram Hill formation on the east limb of the Spring Hill synform from pelitic and quartzitic schists. Sample V634A contains garnet, muscovite, quartz, minor biotite, staurolite porphyroblasts with chloritoid occurring only as inclusions within garnet porphyroblast cores. The inclusion trails within garnet porphyroblasts are dominated by quartz (figs. 5 and 6). The inclusion trails in the rims contain quartz and ilmenite and are inter-grown with staurolite. Abundant monazite is present as inclusions and matrix grains in the cores, medians, rims, strain shadows and matrix of this sample (fig. 5B). Sample V436A contains garnet, muscovite, minor biotite, quartz and locally porphyroblastic plagioclase. The inclusions within garnet porphyroblasts are dominated by quartz in the core and ilmenite in the rim (figs. 7 and 8). Monazite inclusions are present in the core and rim (fig. 7B) and monazite grains are present in the matrix of this sample. The cores and medians of garnet porphyroblasts are rounded to subhedral and are overgrown by stringers of garnet in the rims. Sample V436B contains garnet, muscovite, biotite, quartz and late chlorite. The inclusions within garnet porphyroblasts are dominated by quartz in the core and graphite in the rim (figs. 9 and 10). Monazite grains are present only in the rim of garnet porphyroblasts (fig. 9B). Sample V653 contains garnet, muscovite, minor biotite, quartz and locally staurolite, chloritoid and chlorite that are commonly inter-grown. The inclusions within garnet porphyroblasts consist of quartz (figs. 11 and 12). Monazite is present as inclusions only in the rims of garnet porphyroblasts and as grains in the matrix (fig. 11B). All of the samples contain accessory tourmaline, ilmenite and apatite, and zircon is locally present as inclusions and in the matrix. All of the samples contain garnet porphyroblasts that preserve compositional zoning with several showing complex Ca zoning that is coincident with changes in the microstructure (figs. 5C, 7C, 9C and 11C); all are distinctly texturally zoned (figs. 5A, 7A, 9A and 11A). The metamorphic grade attributed to the rocks in this region peaked at about 730°C and 10.5kb at around 395-385 Ma (Armstrong and others, 1992; Ratcliffe and others, 1992). However, work in progress suggests that the rocks described herein may have achieved higher pressures but lower temperatures than this suggests (Welch, unpublished data).

AGES

Age Determination

Monazite ages were determined using the U-Th-total Pb technique outlined in Montel and others (1996) and Williams and others (1999). This technique is ideally suited to the analysis of monazite grains *in-situ*, which was critical to this study. It has

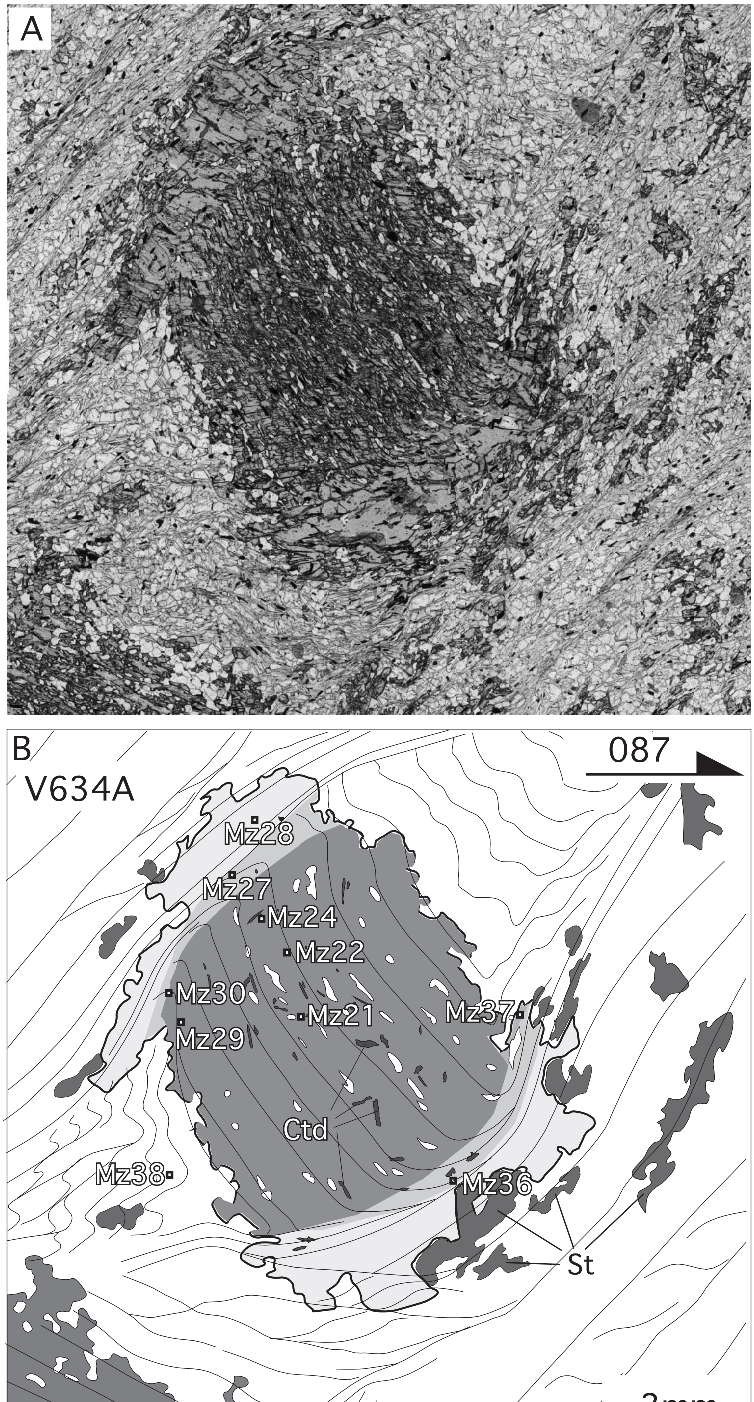

Fig. 5. (A) Plane polarized light photograph of sample V634A. (B) Line diagram of Sample V634A in vertical thin section with its strike (087°) and way up (single barbed arrow) and scale bar shown. The location of monazite grains within foliations preserved as inclusion trails in the cores and rims of garnet porphyroblasts and in the matrix are shown in (B). This sample contains FIA set 1 preserved within the foliation across the core, set 2 within in the curvature of the core foliation, set 3 in the median and set 4 in a portion of the outermost rim. Monazite ages range from 431 Ma to 366 Ma. Grain Mz38 lies in the strain shadow of the porphyroblast core.

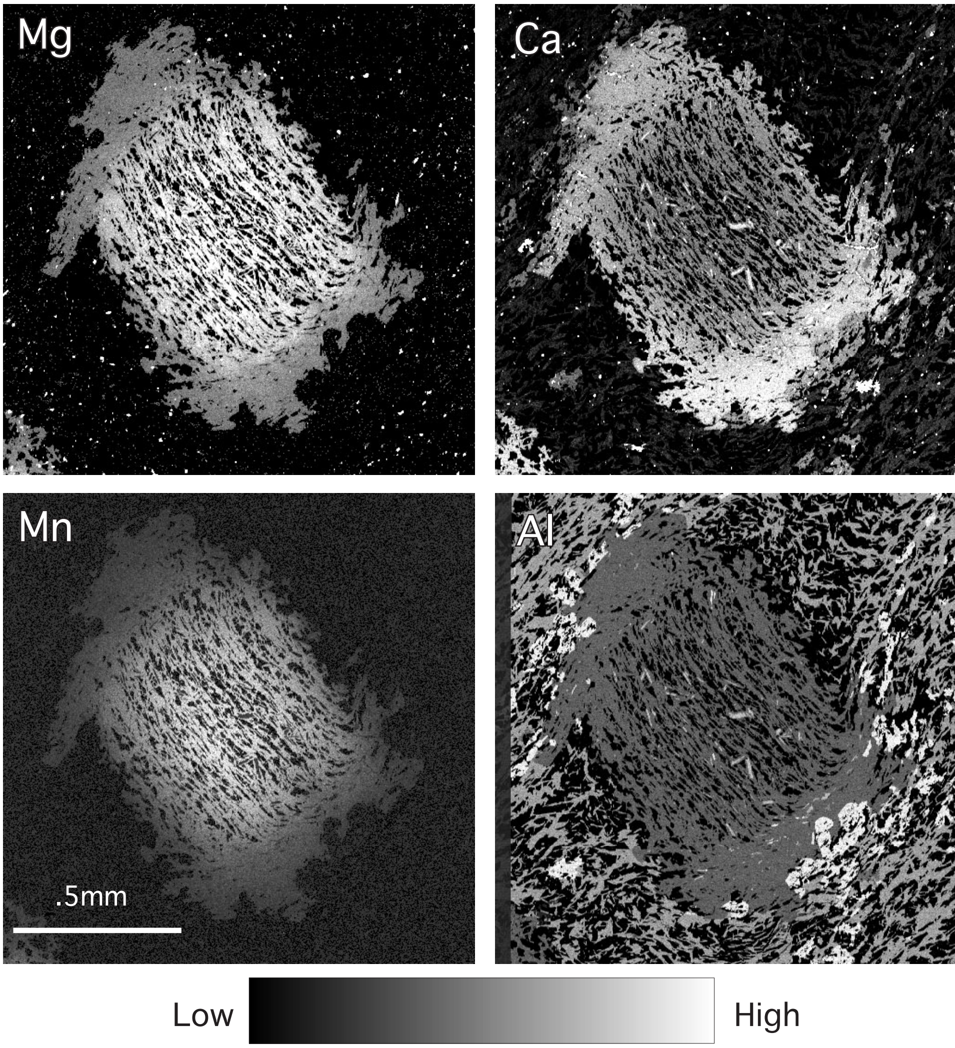

Fig. 5. (C) Mg, Ca, Mn and Al compositional zoning maps of a garnet porphyroblast from Sample V634A shown in figure 5(A) and (B).

been proven to be a viable technique by the dating of monazite grains of known age by these authors. The analyses described herein were obtained from the laboratory of M.L. Williams at the University of Massachusetts, and Williams and others (1999) contains a comparison of monazite grains dated by this and other techniques. Comparisons of the ages obtained with other methods such as SHRIMP and TIMs have shown excellent agreement down to 300 Ma.

Monazite inclusions in garnet are very difficult to identify optically so grains were identified using back-scattered electron imaging and spot checked with EDS. Compositional maps of U, Th, Y and Pb were obtained for all monazite grains to be analyzed to check for multiple growth events using the methods outlined in Williams and others (1999). An example of a set of compositional maps for sample V436A is shown in figure 13. Spot analyses were collected for all compositional domains in a given grain. A

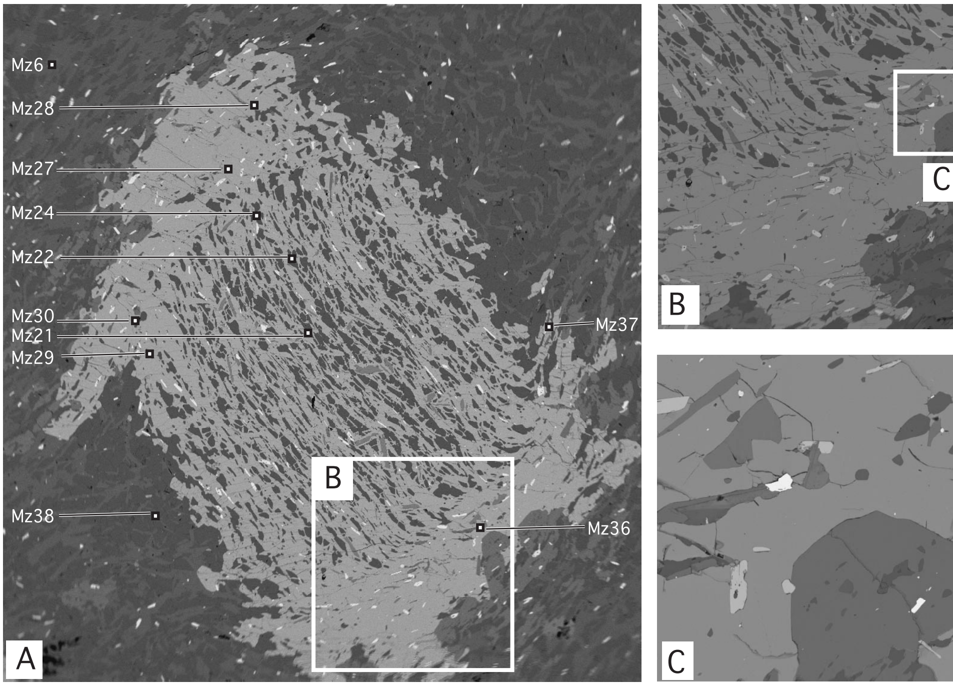

Fig. 6. Back scattered electron images showing location of monazite grains dated (ages given in table 2). (B) and (C) show details of boxed area in (A) regarding the location of grain Mz36. This grain lies on the boundary between the curved core foliation where stage 3 differentiation has occurred and the stage 4 differentiated crenulation cleavage. It has maintained the core age presumably because it deformed (its long axis lies at about 45° to the foliation in the core) but did not recrystallize during the stage 3 of crenulation development associated with FIA set 3.

number of analyses were collected for each grain, or compositional domain in each grain, so that an average age could be calculated (for example, fig. 8B). The point analyses and compositional maps were collected on a Cameca SX-50 in the Department of Geological Sciences at the University of Massachusetts. Grains were analyzed with beam conditions of 15kv and 100nA and 900 second count times.

For each monazite grain dated a mean age was calculated from several analyses (for example, all the analyses in table 1 for the monazite grain shown in fig. 8B). Two ages were calculated for grains with complex zoning where such variation was apparent. A standard deviation and a standard error were calculated for those analyses. This data for each grain from each sample are reported in table 2 at the 1 sigma level of confidence. A normal distribution probability curve was calculated for the mean and standard deviation of each monazite grain. These data are plotted as the small non-grayed curves for each sample in figure 14. A total sum probability curve was then calculated for each sample from these curves. This curve is simply the sum of all of the smaller curves and does not include the grayed curves mentioned below. This was done to see if multiple ages could be seen for the different FIAs when the data were accumulated together rather than just examined in terms of their microstructural location relative to foliations in the core, median and rim.

Each graph in figure 14 also contains weighted average ages with error ranges. These weighted average ages were calculated at the 2 sigma level of confidence for all the monazite grains separated according to FIA and whether they lie in the core, median or rim of a given garnet porphyroblast, or the matrix. They are also plotted on the graphs as the gray shaded curves.

Foliations, FIA Sets and their Monazite Ages

Sample V634A contains FIA set 1 as the axis of the crenulated cleavage lying between the differentiated crenulation cleavage seams preserved as the inclusion trails in the core. The sample contains FIA set 2 as the axis of curvature of the foliation in the core. It also contains FIA set 3 defined by the differentiated crenulation cleavage at stage 3 and stage 4 in the median inclusion trails and FIA set 4 in part of the rim. Monazite grains are present in every microstructural position within garnet porphyroblasts as well as within the matrix (figs. 5B and 6). The probability distribution for all monazite grains dated in this sample is shown in figure 14A and indicates four peaks in the distribution. These coincide with the ages calculated from the weighted averages for monazite grains in the core median, rim and matrix at 424±2Ma, 405±6Ma, 386±6 and 366±4 Ma and which are shown in figure 14 as gray shaded curves. The progressively younger age of the monazite grains from core to rim is readily apparent.

Sample V436A contains FIA set 3 in the core of garnet porphyroblasts and set 4 in the rims. Monazite grains are present in the cores and rims of these porphyroblasts as well as in the matrix (figs. 7B and 8) and their ages range from above 390 Ma in porphyroblast cores down to around 321 Ma in the matrix. The probability distribution for all monazite grains dated in this sample is shown in figure 14B and indicates three peaks in the distribution. These coincide with the ages calculated from the weighted averages for monazite grains in the core and rim at 391±8 Ma and 366±6 Ma respectively, which are shown in figure 14B as gray shaded curves, and 321±23 Ma in the matrix. The progressively younger age of the monazite grains from core to rim to matrix is readily apparent.

Samples V436B and V653 contain FIA set 3 in the core of garnet porphyroblasts and FIA set 4 in the rims, but monazite grains are only present in the rims. Sample V436B yielded ages of 349±8 for monazite grains in the rim and matrix as well as an anomalously old age of 416±14 Ma (figs. 9B, 10 and 14C). This ellipsoidal shaped monazite grain (grain Mz1 in fig. 10) lies in the rim of the garnet porphyroblast at a high angle to the surrounding inclusion trails. It has the same orientation as the foliation defined by inclusion trails in the core (fig. 10). Sample V653 yielded an age of 350±11 Ma for monazite in the rims (figs. 11B and 12). Monazite grains are also present in the matrix; the youngest were 316±9 Ma.

The Combined Age Data Set

An analysis of all forty-seven ages of individual monazite grains obtained from these samples, shown in figure 15A via a probability density curve, produced a series of 5 peaks at 425 Ma, 400 Ma, 387 Ma, 365 Ma and 350 Ma. These can be compared with the 5 peaks determined from the weighted average ages based on FIA set and microstructural location (see below) combined for all samples, shown in figure 15B, at 425 Ma, 405 Ma, 387 Ma, 367 Ma and 352 Ma.

INTERPRETATION

Foliation Development and Preservation as Inclusion Trails

Quartz, graphite, muscovite and biotite are the minerals in pelitic rocks that commonly define the matrix foliation. Porphyroblasts generally overgrow and preserve quartz and graphite from the matrix as inclusion trails but not muscovite and biotite. Possibly the latter minerals are rarely preserved because they tend to be used by the reactions from which the porphyroblastic phases grow, either directly, or indirectly in Carmichael-type exchanges. Every time a new foliation forms to stage 3 or more of

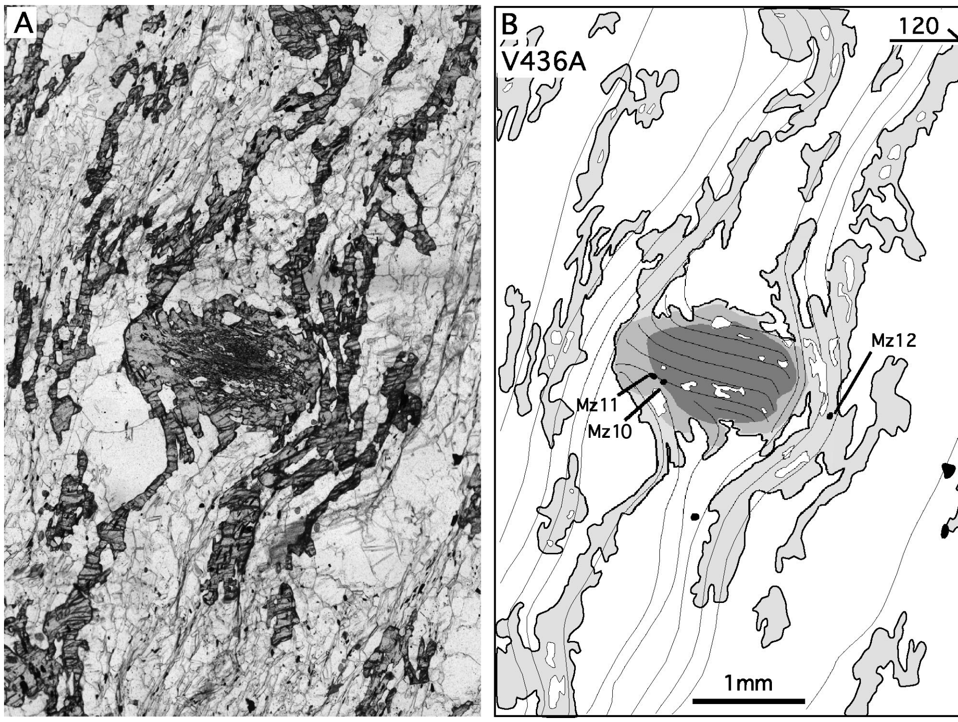

Fig. 7. (A) Plane polarized light photograph of a garnet porphyroblast from Sample V436A. (B) Line diagram of sample V436A in a garnet porphyroblast in a vertical thin section with its strike (120°) and way up (single barbed arrow) and scale bar shown. The location of monazite grains within foliations preserved as inclusion trails in the cores and rims of garnet porphyroblasts and in the matrix are shown in (B). This sample contains FIA set 3 in the cores and FIA set 4 in the rims.

differentiated crenulation cleavage development (Bell, 1986; fig. 16A-E), the matrix reconstitutes as deformation and metamorphism take place, resetting any isotopic clocks present in minerals such as monazite and zircon that are affected by progressive shearing (for example, Page and Bell, 1986). This reconstitution involves deformation, recrystallization, dissolution and solution transfer and removal of non-platy minerals, such as quartz, from zones of progressive shearing (cleavage seams), during crenulation cleavage development (fig. 16B, C, D; Bell & Cuff, 1989) or reactivation of bedding (Bell, 1986). It also involves recrystallization of the phyllosilicates left behind in the cleavage seams (Bell and Cuff, 1989). Those minerals dissolved may nucleate and grow again in zones of progressive shortening, most obviously in strain shadows adjacent to porphyroblasts, or as fibers, but also generally within the matrix (for example, Williams and others, 2001). Generally, some material is removed entirely from the local system (Bell and Cuff, 1989).

Monazite Behavior During Foliation Development

The phase relations of monazite are not well understood but it grows as a metamorphic mineral in amphibolite facies rocks (Parrish, 1990; Smith and Barreiro, 1990; Lanzarotti and Hanson, 1996). Our data demonstrates that successively younger generations of foliations preserved from the cores to rims of porphyroblasts as inclusion trails contain progressively younger monazite grains, with even younger grains commonly present in the matrix foliation (figs. 5 to 12). There are two possible

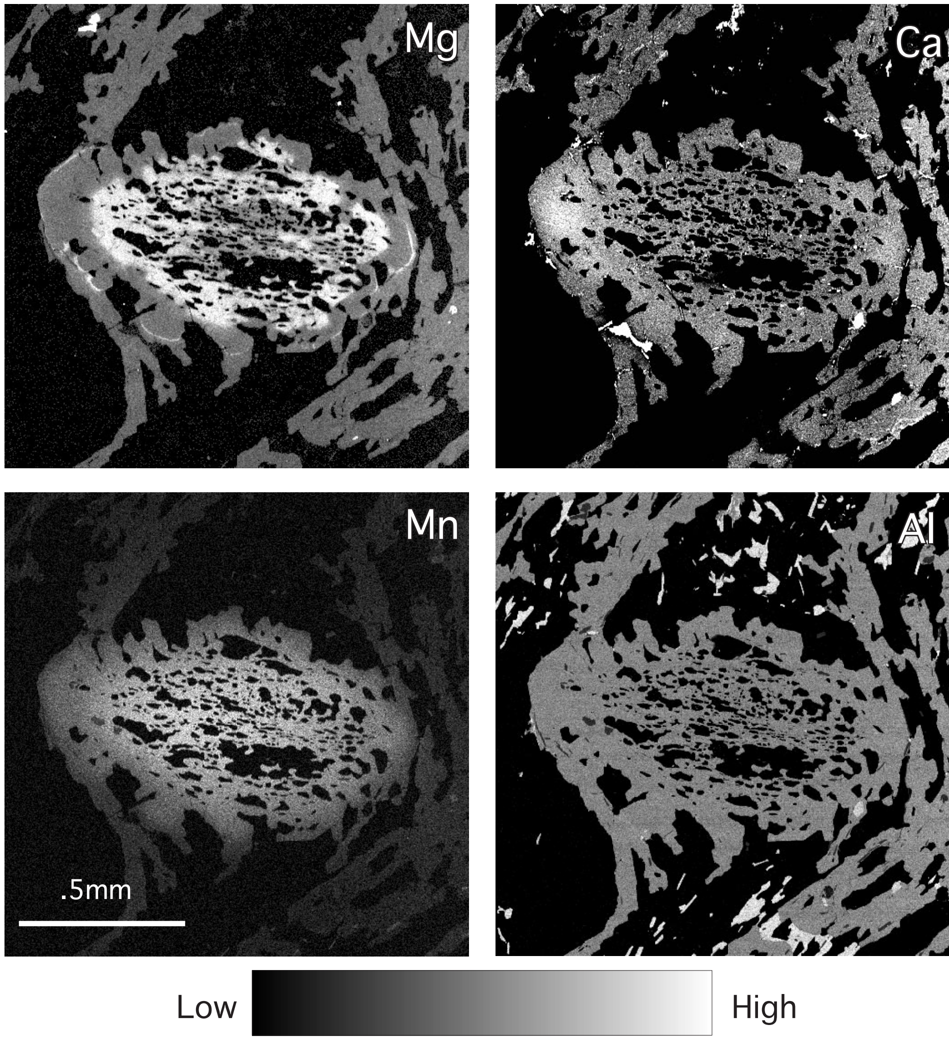

Fig. 7. (C) Mg, Ca, Mn and Al compositional zoning maps of a garnet porphyroblast from Sample V436A shown in figure 7(A) and (B).

explanations for the behavior of monazite that would explain this progressive reduction in ages each time a new foliation forms (see also Shaw and others, 2001; Williams and Jercinovic, 2002). Each time a new foliation has formed the older monazite grains preserved in porphyroblasts cores have been plastically deformed and recrystallized, or they have been plastically deformed on their margins, dissolved, undergone solution transfer to a new site and nucleated and grown as new grains. The latter process would certainly reset the internal radiogenic clock that results from the decay of U and Th. The former process would probably reset the radiogenic clock as well, because the movement of high angle grain boundaries through the monazite grains as they recrystallized should release any Pb that had built up from radiogenic decay. For the rocks described herein monazite has behaved in this manner during a P-T-t history involving a range in temperature from 560° to well over 600°C and pressures ranging from 6 to well over 11 kbars (Welch, unpublished data). This behavior makes it an ideal

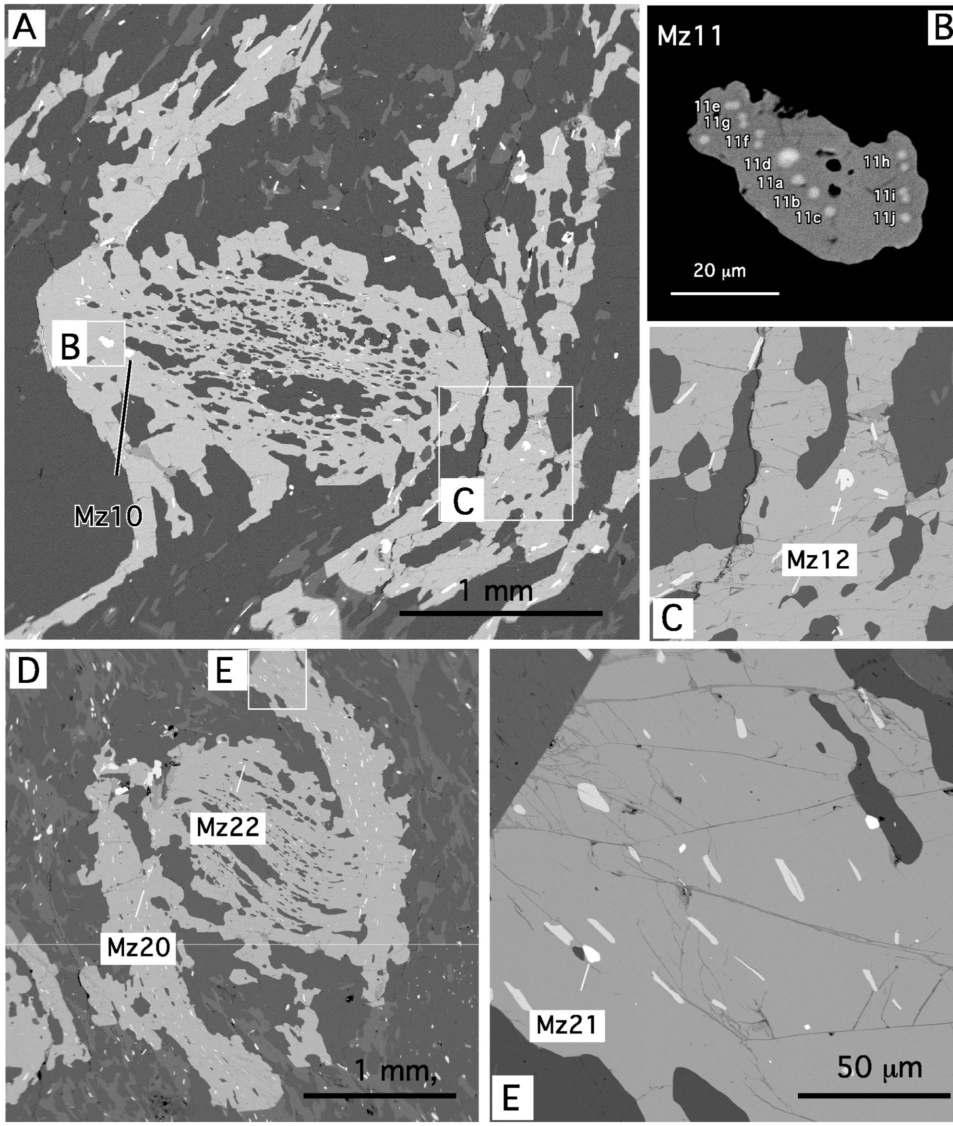

Fig. 8. Back scattered electron images showing garnet porphyroblast from fig. 7A, enlargement of a monazite grain (B) from within boxed area marked in (A) showing location of each analysis (analyses given in table 1), plus location of other monazite grains in this (C) and other (D and E) porphyroblasts.

mineral for dating foliations that accompany the growth of many of the most common porphyroblastic phases in pelites. All the lead resulting from the radioactive decay of uranium and thorium after the foliation formed, can be measured on a microprobe and an age can be calculated (Montel and others, 2000; Williams and Jercinovic, 2002).

Monazite Microstructural Relationships

Some uncommon monazite microstructural relationships that we have observed throw further light on the behavior of this mineral during foliation development. Monazite can grow within a developing foliation over minerals such as ilmenite that define an earlier formed foliation and preserve them as inclusions as shown in figure 12D. Relatively early formed monazite grains can be preserved in the strain shadow of a porphyroblast and remain protected from the effects of subsequent deformation and younger foliation development (for example, grain Mz38 in fig. 5B). Some monazite grains have been affected by the development of a younger foliation but have not fully recrystallized and retain the age of an older foliation in their cores (for example, grains Mz10 and Mz12 in fig. 8, and Mz4 in Sample V634A, table 2). Locally, a monazite grain (for example, grains Mz27 in fig. 5B, Mz11 in fig. 8A, B and Mz1 in fig. 10) preserves an anomalously old age in the median, rim or matrix of a porphyroblast where the other monazite grains have much younger ages. Where this occurs, the monazite grain is quite elongate and lies at a high angle to the surrounding foliation preserved as very fine inclusion trails in the surrounding porphyroblast or in the matrix. These elongate grains are similar in size and lie exactly parallel to those inclusions that define the foliation in the core of the porphyroblast. We interpret that they are relict core grains that have survived the effects of subsequent foliation development because they crystallographically lay in an orientation where they remained strong relative to the deforming forces and did not plastically deform. This behavior prevented recrystallization and dissolution (Bell and others, 1986; Bell and Cuff, 1989). Mancktelow (1981) documented this phenomenon in quartz and showed that some grains have their C-axes in orientations whereby they are very strong relative to the superimposed forces and can survive the effects of intense deformation and maintain their original orientation. Without internal plastic deformation, recrystallization or dissolution, solution transfer and nucleation and growth are prevented (Bell and Cuff, 1989) and resetting of the age does not occur. We interpret that the age determined from these grains provides an age for the core foliation. Monazite grain Mz36 in figure 6 is similar to the 3 grains just described but we interpret that it has undergone some internal plastic deformation because it has been rotated 45° relative to the foliation in the core. Yet it too has maintained a core age. We infer that the internal plastic deformation was insufficient to cause this grain to recrystallize. As a result its age is not reset. The latter four of the five monazite microstructural features described herein bring into focus the possibility of inheritance of older monazite ages (for example, Harrison and others, 1999) and lead loss (Smith and Giletti, 1997). The Cram Hill formation from which these samples were taken is Ordovician in age. The oldest monazite inclusion that we have dated is 430 Ma and therefore too young to be an inherited age unless intra-crystalline diffusion has occurred. The common preservation of compositional zoning in monazite (fig. 13) suggests that intra-crystalline diffusion did not occur or was very limited and this is supported by the succession of ages from core to rim of the porphyroblasts and the consistency of these ages for successive FIA sets from sample to sample.

Interpretation of the Ages Obtained from Each Sample

Figure 14 shows for each sample the probability curve for the age of each monazite grain dated, this curve resulting from the sum of all of the individual monazite age curves. It also shows the weighted average age calculated for monazite grains according to the FIA and microstructural setting (porphyroblast core, median or rim and the matrix) and curves (shaded in gray) defining these weighted average ages. Figure 5 shows a garnet porphyroblast from sample V634A and contains a large range of monazite ages where the microstructural and FIA setting of the grains enable the interpretation and dating of a long history of FIA development. The ages of the monazite grains within the foliation crossing the core are 434, 431 and 430 Ma. This foliation is a differentiated crenulation cleavage at stage 4 of development (fig. 16) with the remains of the crenulated cleavage from which it formed preserved in Q-domains. The axes of the crenulated cleavage belong to FIA set 1 and we interpret

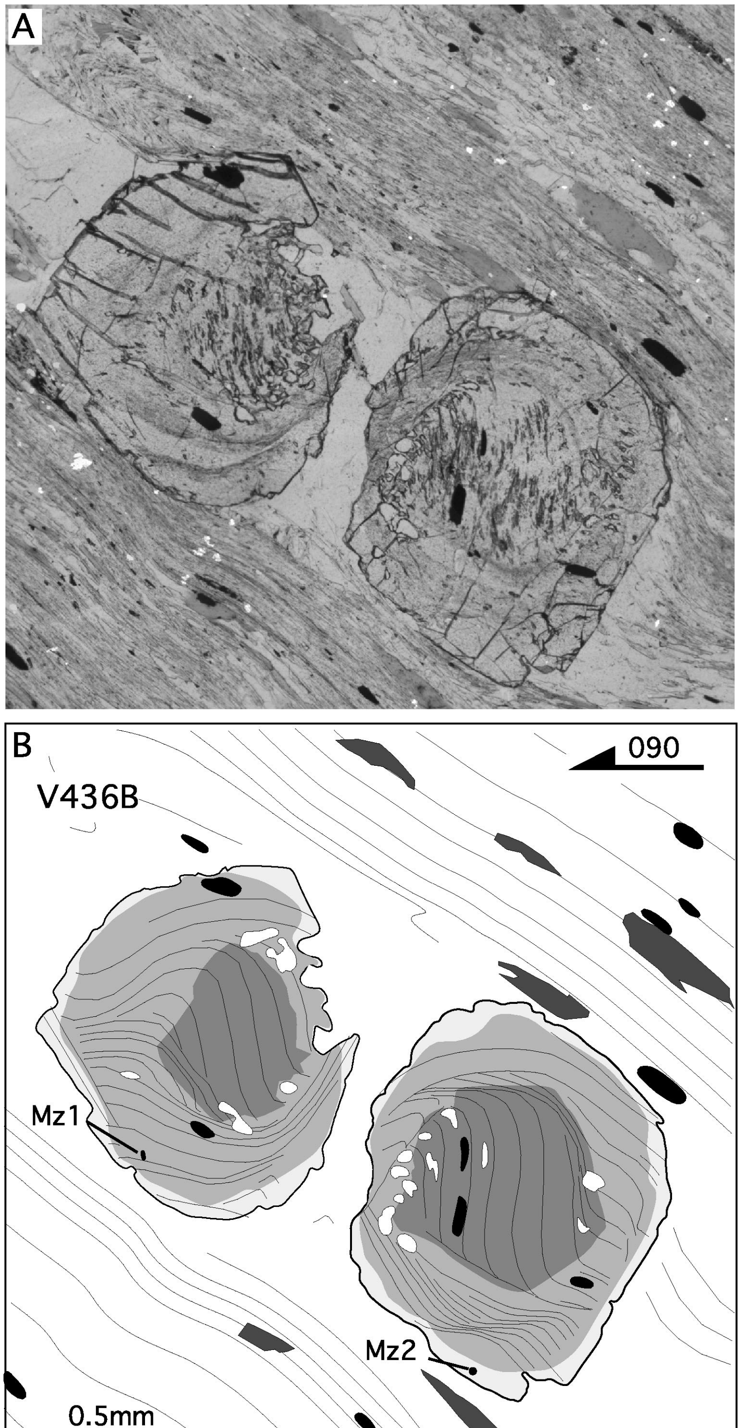

Fig. 9. (A) Plane polarized light photograph of a garnet porphyroblast from Sample V436B. (B) Line diagram of a garnet porphyroblast from Sample V436B in a vertical thin section with its strike (090°) and way up (single barbed arrow) and scale bar shown. The location of monazite grains within foliations preserved as inclusion trails in the median of the garnet porphyroblasts is shown in (B). (The monazite grain Mz1 is too small to see in the photograph and so an ellipse with the same orientation is shown in this line diagram at its location). This sample contains FIA set 3 in the core of garnet porphyroblasts and FIA set 4 in the rims, but monazite grains are only present in the porphyroblast rims and the matrix.

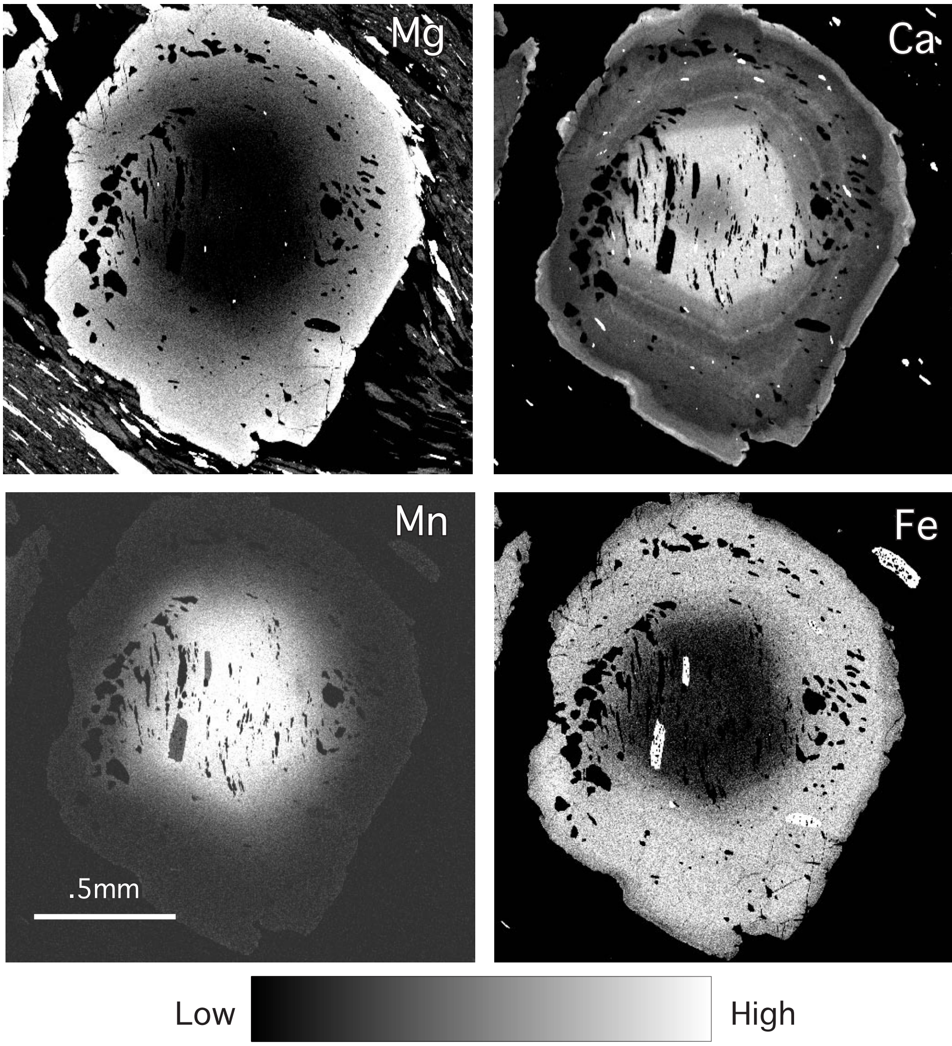

Fig. 9. (C) Mg, Ca, Mn and Al compositional maps of a garnet porphyroblast from Sample V436B shown in 9(A) and (B).

the monazite ages in the core to have formed during the development of FIA set 1. The core of the porphyroblast formed during FIA set 2 (fig. 17A). The 424 Ma ages at locations Mz37 and Mz38 (fig. 5B) formed in the strain shadow of the core after it developed and provide an indication of the age of FIA set 2. The 400 Ma (432 Ma is relic of core) and 402 Ma ages in the median of the porphyroblast are preserved within a stage 3 differentiated crenulation cleavage (fig. 16B, C) that was the first foliation that formed during FIA set 3 in this sample (fig. 17B). This portion was subsequently overgrown by garnet (fig. 17C). Shear during a younger event formed a truncational differentiated crenulation cleavage at stage 4 of development (fig. 16D, G, J) against the median containing monazite grains dated at 379 Ma, 398 Ma (the 413 Ma for Mz27 is a relic of core grain as described earlier; fig. 17D). Similarly, overgrowth of a younger gently dipping differentiated crenulation cleavage by garnet occurred during further

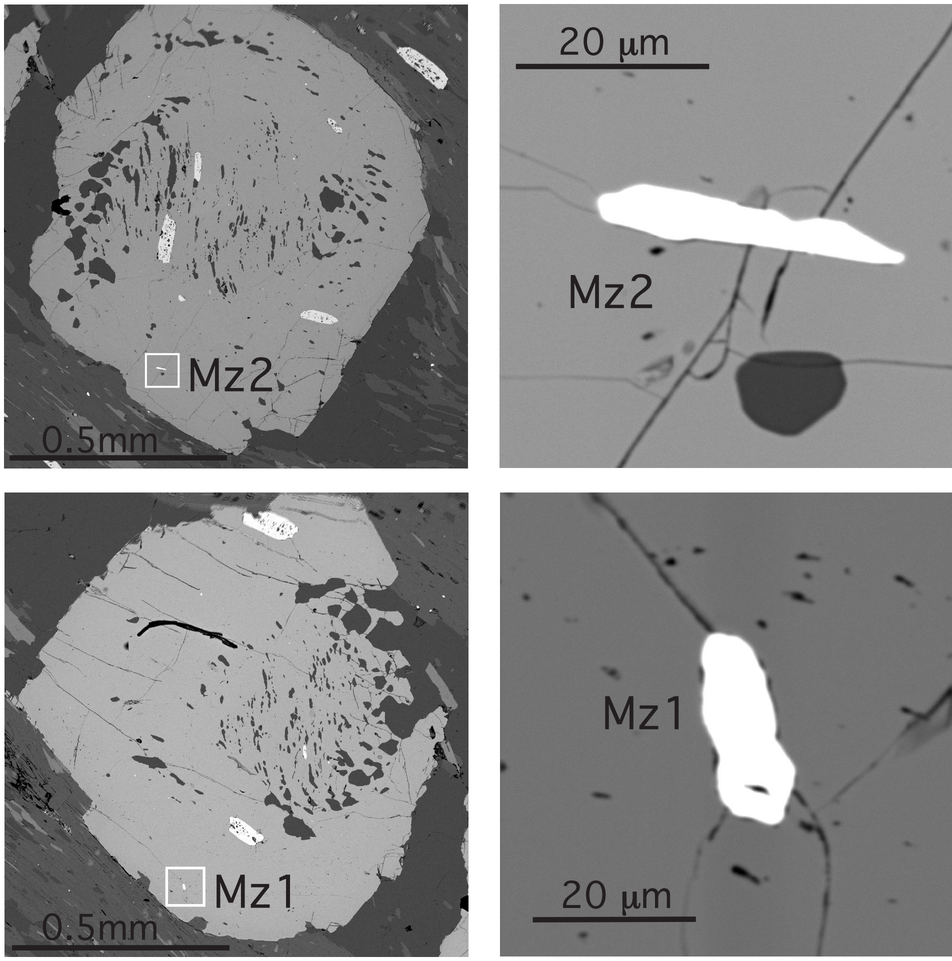

Fig. 10. Back scattered electron images showing garnet porphyroblasts from figure 9A and the location of two monazite grains that were dated. Mz1 lies oblique to the foliation containing it and parallel to the foliation in the core.

development of FIA set 3 (fig. 17E). The matrix contains monazite grains dated at 366 Ma. The latest visible differentiated crenulation cleavage in the matrix was overgrown by staurolite porphyroblasts during a very, weakly developed crenulation event that causes shallow microscopically visible deflections through the staurolite grains and defines FIA set 4. This was the only younger event recorded in this rock and the matrix appears to have not been affected by any other events.

Figure 7 shows a garnet porphyroblast from sample V436A that preserves a microstructurally visible core, median and rim, based on inclusion trail density and composition, associated with FIA sets 3 (core) and 4 (median and rim). The porphyroblasts in this sample contain monazite age relationships relative to the microstructural setting that reveal significant characteristics of the behavior of monazite during foliation development. Table 2 and figure 8 show that the cores of these porphyroblasts contain monazite grains dated at 392 and 393 Ma. Garnet overgrew these cores during the development of FIA set 3 and these grains formed before or during this period; based on sample V634A described above, we interpret that the foliation containing these grains formed during FIA set 3. Monazite grains Mz10 and Mz12 occur in the median and rim respectively, where the inclusion trails define foliations that formed during the development of FIA set 4, and both grains contain an older core at 390 and 402 Ma and a younger rim at 364 and 373 Ma respectively. The older core is interpreted to be remains of the foliation preserved in the porphyroblast cores. The Mz11 grain has the same age and orientation as the monazite grains in the porphyroblast cores (fig. 8A, B). This suggests that it was not significantly affected by plastic deformation during the development of foliation in the median. As reported above, it appears to have remained in a strong orientation relative to the stress field. Figure 8D, E shows monazite grains Mz20 and Mz21 that formed during the development of the rim at 358 and 363 Ma (the younger ages from Mz20 are regarded as anomalous). The younger rim is interpreted to be the age of development of the foliation in the median and the rim for Mz20 and Mz21 respectively, both of which developed during FIA set 4.

Figures 9 and 10 show garnet porphyroblasts from sample V436B that preserve a microstructurally visible core, median and rim, based on inclusion trail density and composition, which define FIA set 3 in the core and FIA set 4 in the median and rim. No monazite grains were found in the core. However, a few grains were found in the median with ages of 362, 357, 349 and 348 Ma (for example, fig. 9). One monazite grain, Mz1 that lies in the median, is elongate at a high angle to the foliation surrounding it but parallel to that within the core (fig. 9). This grain has an anomalously old age of 416 Ma and we interpret that it is a relic of the latter foliation, as mentioned in the section above. Consequently, it could have formed before or during FIA set 3. A few grains in the matrix have younger ages of 338 and 337 Ma and are interpreted as providing an age for the matrix foliation.

Figures 11 and 12 show garnet porphyroblasts from sample V653 that preserve a microstructurally visible core and rim, based on inclusion trail density and composition, and defining FIA set 3 in the core and FIA set 4 in the rim. No monazite grains were found in the core. However, monazite grains were found in the rim. These monazite grains have ages of 359, 358, 358 and 354 Ma with two anomalously younger ages at 345 and 309 Ma. The few monazite grains observed in the matrix have younger ages ranging from 350 and 347 to 327 and 319 Ma. The potential significance of this spread of matrix ages is discussed below.

Significance of Monazite Ages for the Episodicity of Porphyroblast Growth Reactions

The progressively younger ages of monazite grains preserved in the succession of foliations from the core to rims of porphyroblasts in figures 5 to 12 and 14 reveal 70 million years of episodic regrowth of garnet at intervals up to 20 million years apart. The progressively younger monazite grains outside of the porphyroblast cores occur in foliations that have formed against successively grown portions of the porphyroblast rims (for example, fig. 16F-J). The inclusion trail geometries suggest that each phase of porphyroblast growth occurred early in a deformation event and that after growth ceased, the foliation in the matrix intensified against the porphyroblast rim (for example, fig. 16F-J). These ages provided quantitative confirmation of the episodicity of porphyroblast growth that has been recognized microstructurally for over a decade (Bell and Johnson, 1989; Bell and Hayward, 1991; Spiess and Bell, 1996). Some porphyroblast growth reactions stopped and started several times over a period of 70 million years without necessarily going to completion.

Foliation Ages Versus Porphyroblast Age

As described above, we interpret that the ages of monazite grains within a foliation generally reveal when that foliation formed. Therefore, we argue that monazite grains

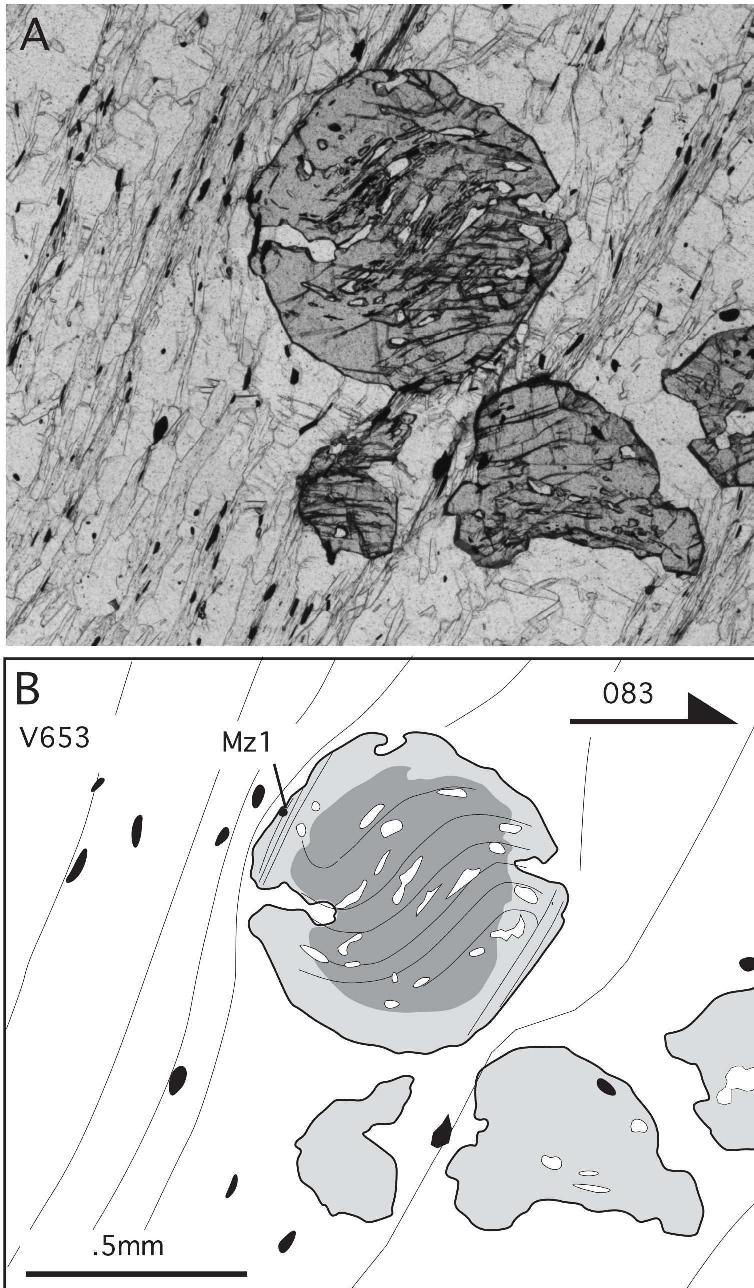

Fig. 11. (A) Plane polarized light photograph of a garnet porphyroblast from Sample V653. (B) Line diagram of a garnet porphyroblast from Sample V653 in a vertical thin section with its strike (083°) and way up (single barbed arrow) and scale bar shown. The location of monazite grains within foliations preserved as inclusion trails in the cores and rims of garnet porphyroblasts and in the matrix are shown in (B). This sample contains FIA set 3 in the core of garnet porphyroblasts and FIA set 4 in the rims, but monazite grains are only present in the porphyroblast rims and the matrix.

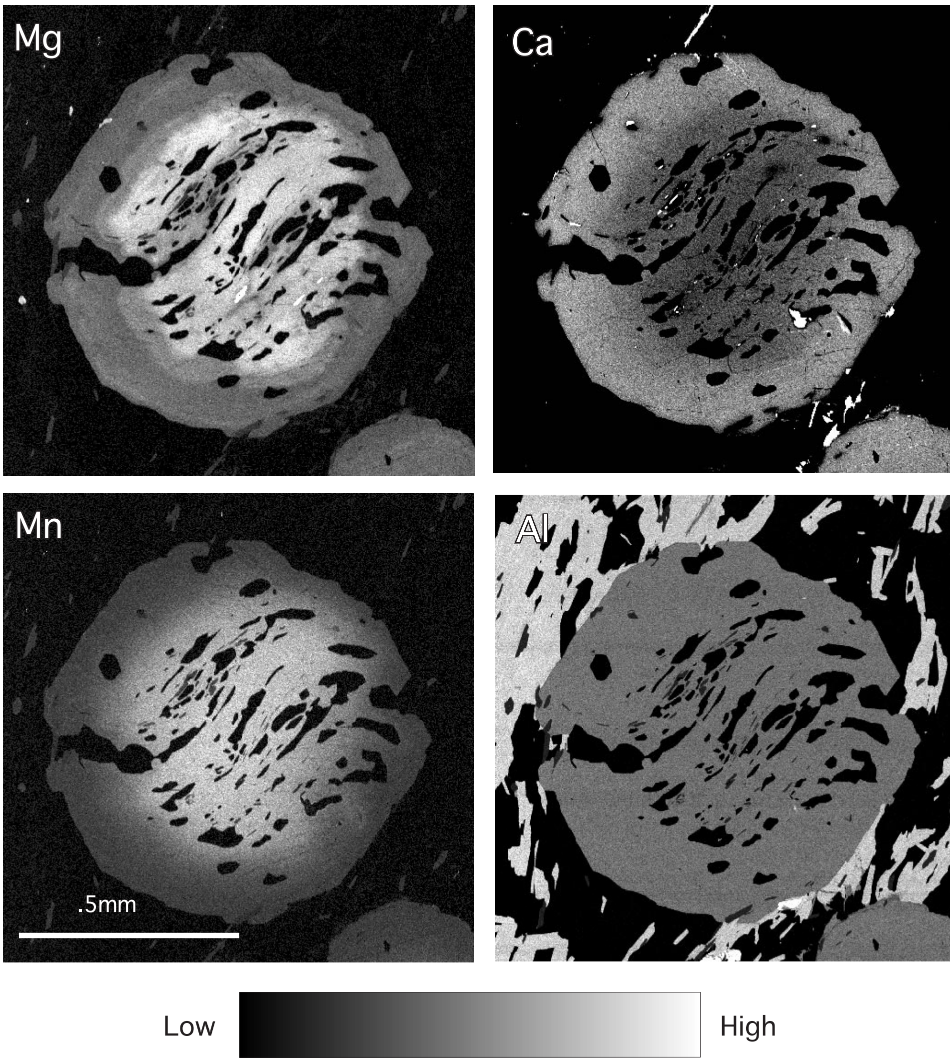

Fig. 11. (C) Mg, Ca, Mn and Al compositional zoning maps of a garnet porphyroblast from Sample V653 shown in figure 11 (A) and (B).

occurring as simple inclusion trail geometries cannot be used to determine the absolute age of the porphyroblast encompassing that foliation. They simply tell us that the porphyroblast grew after the formation of the monazite grain. However, once a porphyroblast has overgrown the foliation preserved in its core, new foliations commonly form against its rim during younger deformations (fig. 16G, I, J). Incorporation of these younger foliations within the porphyroblast during later phases of growth is also common, and generates more complex trail geometries such as spiral and staircase shapes (fig. 16F, H, J; for example, Bell and Johnson, 1989; Bell and Hayward, 1991). This process of foliation development against a porphyroblast rim and subsequent incorporation by more porphyroblast growth can be repeated many times. Where this occurs it allows bracketing of the time of growth of portions of the porphyroblast if monazite grains are preserved as inclusions in each foliation. For this

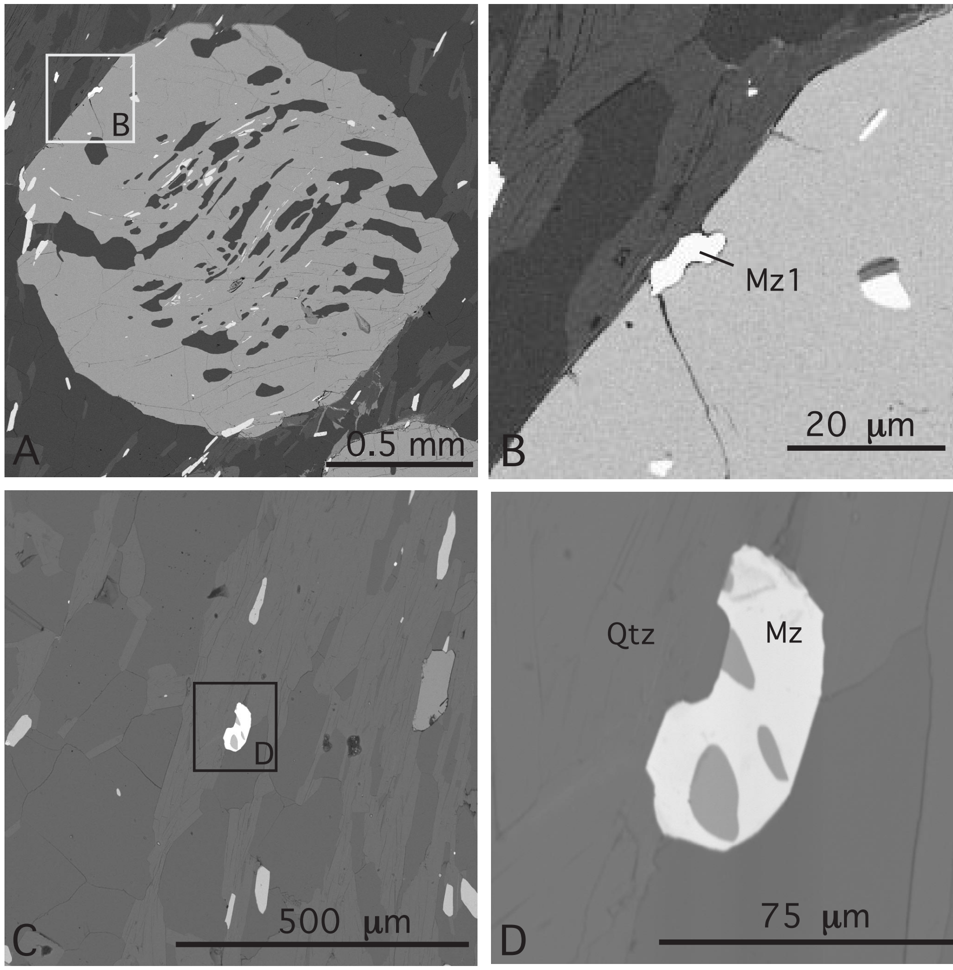

Fig. 12. Back scattered electron image of garnet porphyroblast shown in figure 11A, showing enlargement of monazite grain (B) in location marked in boxed area in (A), a monazite grain in the matrix (C) and an enlargement of this monazite grain (D) as it contains rutile inclusions that define a foliation.

part of Vermont as many as seven such phases of growth have been documented in garnet porphyroblasts (for example, Bell and Johnson, 1989). Sample V634A provides an excellent example of the process just described. Foliation in the core contains monazite grains dated at 424±2.4 Ma (figs. 5, 6 and 14). Therefore the garnet overgrowing the core grew after that date (fig. 17A). Differentiation associated with curvature on the edge of the core ranges in age from 405±6 to 386±6 Ma. Therefore the garnet in the core grew between 424±2.4 and 405±6 Ma (fig. 17B). Monazite inclusions in the stage 3 differentiated cleavage (fig. 16) on the edge of the core are dated at 405±6 Ma and were overgrown by garnet before the truncational stage 4 crenulation cleavage (fig. 16) formed that contains monazite inclusions dated at 386±6 Ma (fig. 17C). Therefore the garnet overgrowing the edge of the core formed after 405 Ma, but before 386 Ma (fig. 17C). The matrix contains monazite grains dated at 366±4 Ma. Therefore, garnet in the rim (fig. 17E) grew before 366 Ma and after 386 Ma. A gently dipping portion of the outermost rim contains garnet that grew during

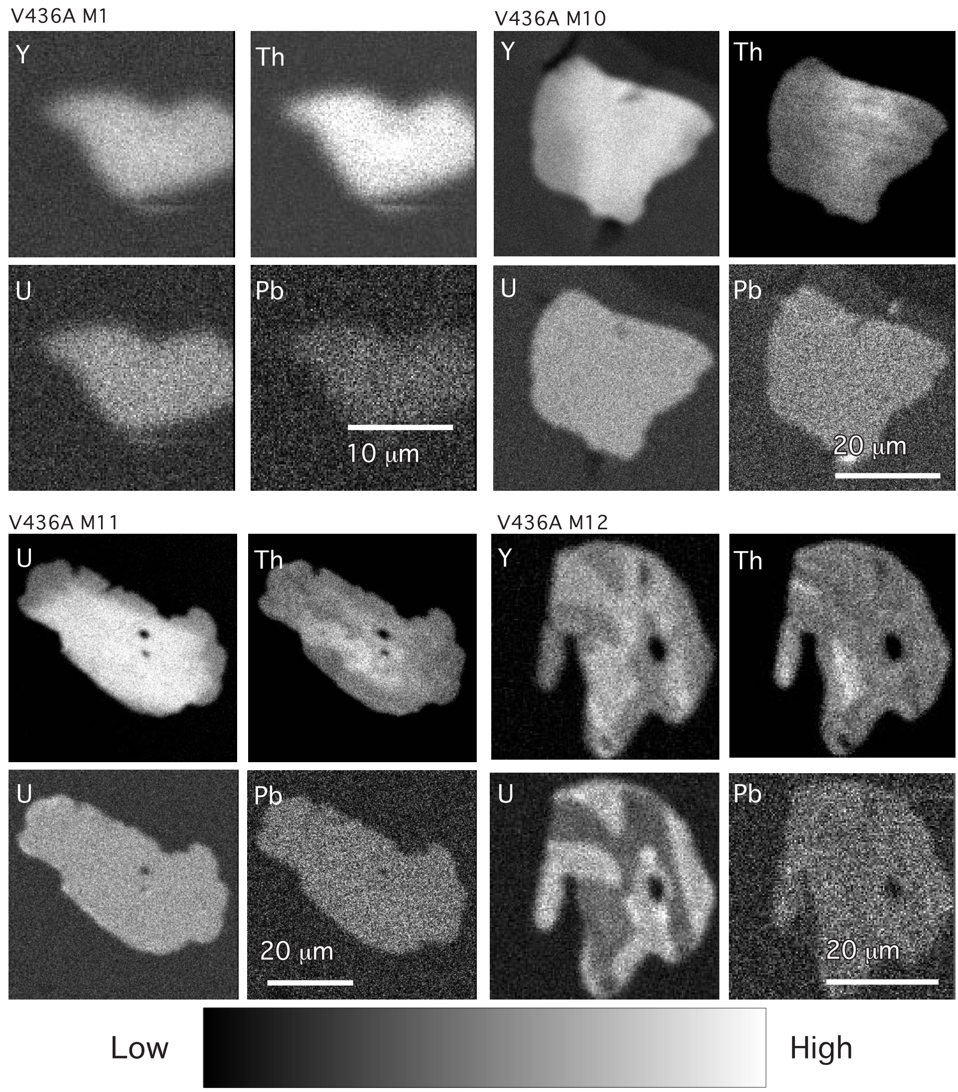

Fig. 13. Compositional maps of four monazite grains from Sample V436A showing their Y, Th, U, and Pb contents.

FIA set 4 around or after 386 Ma (fig. 17F). Similar but younger histories are recorded by the other samples.

The Correlation of Ages with FIA Trends

The progression in monazite ages with the succession of FIA sets is consistent from sample to sample. It provides independent and quantitative confirmation of the validity of the correlation of FIA sets described by Bell and others (1998), which was based on consistent core to rim changes in FIA trends over a 4375 square kilometer region. It suggests that once a succession of FIA trends has been defined and dated, they can be used as a guide to the age of the deformation and metamorphism in other samples from that region. Thus, successive sets of FIAs may provide a new and powerful

Table 1

Shows for one monazite grain numbered Mz11 from sample V436 the location of each analysis (shown on grain in fig. 8A, B), the Y, Th, Pb and U analyses obtained, and the calculated age

Analysis	Y	Th	Pb	U	Age
V436A-11a	11771	48799	1106	4305	386
V436A-11b	11811	52215	1156	4260	384
V436A-11c	10730	42330	1005	3910	400
V436M-11h	7208	34171	883	4074	410
V436M-11i	7466	30647	796	3822	406
V436M-11j	8673	32750	915	4152	434
V436M-11d	4683	30341	802	3934	411
V436M-11f	9076	33244	848	4032	401
V436M-11g	10564	32273	814	3913	395

means of correlating and dating deformation and metamorphism across and along an orogen. Since the orientations of successive FIAs ought to directly reflect changes in the relative direction of plate motion (Bell and others, 1992; 1995; 1998), we possibly now have the means of accessing and dating the history of plate motions that have formed orogens older that the 170 Ma age of the oldest oceans.

FIA Versus the Matrix Ages

This data from 180 analyses of forty-seven monazite grains from four different samples suggests that switches in trend for the consistent FIA succession recorded by Bell and others (1998) for Vermont from SW-NE to W-E, W-E to NNW-SSE and NNW-SSE to SSW-NNE occurred around 425 Ma, 400 Ma and 375 Ma respectively. However, we interpret that deformation and metamorphism occurred throughout this period of time. We suggest that the peaks in the total distribution of ages shown in figure 15 may broaden as more samples across the region containing monazite grains are discovered and dated. However, a peak in the distribution of ages within each FIA set may still be present after hundreds of samples have been dated. This would result from a lag in the pervasiveness of deformation that ought to occur after each change in the relative direction of plate motion indicated by a change in FIA trend (Bell and others, 1998). The matrix preserves ages ranging from 360 Ma to 320 Ma. All deformation that involves a component of bulk shortening is inherently partitioned across and through the crust into components of progressive shortening and shearing (Bell, 1981). Alleghanian deformation around 300 Ma has been documented in shear zones mantling the Pelham Dome only 60 km to the SSE of this region (for example, Moecher, 1999). The effects of this younger period of orogenesis have propagated a large distance from the boundary with Avalon to the SE and could have affected rocks this relatively short distance further north. The discrete nature of Taconian, Acadian and Alleghanian orogenesis as previously described may disappear as more age information of this type is derived. We interpret that deformation was essentially continuous but heterogeneously distributed from 431 Ma to 349 Ma and possibly to 327 Ma. This is close to covering the full range between the Taconic and Alleghanian orogenies.

TABLE 2

Shows for each monazite grain (numbered, M = Mz in text) dated within each sample (sample number) every age obtained from each grain dated, the location of the grain relative to the core, median and rim of the porphyroblast (where these can be distinguished microstructurally according to successive foliations), the mean of these ages, the standard deviation and the standard error

Monazite	Monazite position	Ages	Mean	Stdev	Std error
V634A					
V634A-M1	median	390 385 389 392 382	388	4	2
V634A-M4rim	rim	389 383 394 380 392	387	4	2
V634A-M4core	rim	415 421	418	7	3
V634A-M6	matrix	360 366 370 368	366	4	3
V634A-M8	median	392 420 387 374 395	394	17	8
V634A-M9	median	397 375 372 405	387	16	8
V634A-M20	median	394	394	N/A	N/A
V634A-M21	core	434 395 405	411	20	12
V634A-M22	core	436 426	431	7	5
V634A-M24	median	407 401 399	402	4	2
V634A-M27	median	418 408	413	7	5
V634A-M28	rim	374 387 377	379	7	4
V634A-M29	median	432 426 434	431	4	2
V634A-M30	median	384 411	398	19	14
V634A-M33	matrix	414 401 408	408	7	4
V634A-M36	median	405 407 387	400	11	6
V634A-M36	median	432	432	N/A	N/A
V634A-M37	median	424 425	425	1	1
V634A-M38	matrix	416 420 435	424	10	6
V436A					
V436A-M1	core	399 385 381 397 399	392	9	4
V436A-M4	rim	390 377 388 374	382	8	4
V436A-M5	core	388 395 376 378	384	9	4
V436A-M10-C	median	399 396 381 384	390	9	4
V436A-M10-R	median	367 353 366 371	364	8	5
V436A-M11	median	434 411 401 395 406 386			
		384 400 410	403	15	5
V436A-M12-C	rim	418 394 404 393	402	12	6
V436A-M12-R	rim	368 375 377	373	5	3
V436A-M25	core	374 388 401 379	386	12	6
V436A-M20-C	rim	374 346 348 362	358	13	7
V436A-M20-R	rim	316 329 301	315	14	8
V436A-M21	rim	359 366	363	5	4
V436A-M22	core	383 403	393	14	10
V436A-M24	matrix	318 347	333	21	15
V436B					
V436B-M1	rim	407 430 410	416	13	7
V436B-M2	rim	358 365	362	5	4
V436B-M3	rim	346 334 354 342 366 342	357	14	4
		370 363 373 361 378 356			
V436B-M4	matrix	342 332	337	7	4
V436B-M6	matrix	342 333 335 345	339	6	3
V436B-M8	rim	346 351	349	4	3
V436B-M9	rim	350 372 335 334	348	18	9
V653					
V653M1	rim	364 329 346 330 363 393	358	22	8
		359 379			
V653M4	matrix	357 344 353 345	350	6	3
V653M5	rim	371 366 347 353	359	11	6
V653M7	rim	362 349 343 382 351 369	358	12	4
		356 354			
V653M21		324 313	319	8	6
V653M23	matrix	313 331 334 330	327	9	5
V653M24	matrix	363 344 326 355	347	16	8
V653M30	rim	348 352 348 332	345	9	4
V653M31	rim	351 357	354	4	3
V653M33	rim	307 316 303	309	7	4

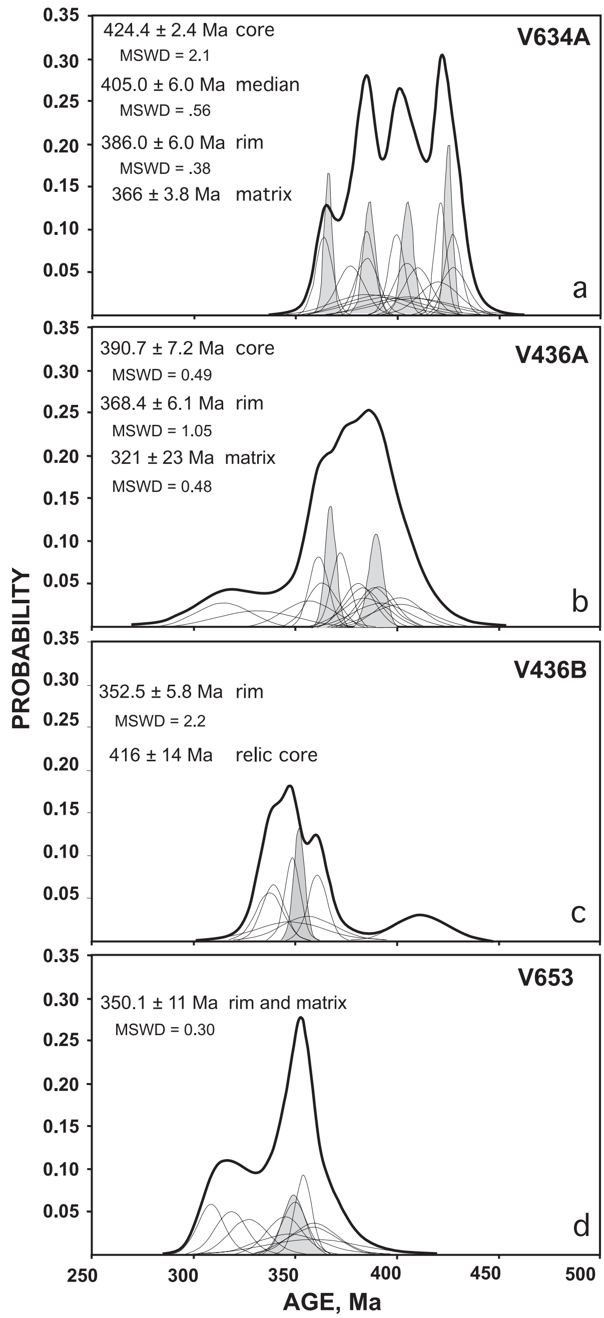

Fig. 14. Graphs for 4 samples showing a normal distribution probability curve (unfilled with fine lines) calculated for the mean and standard deviation of each monazite grain from several analyses. Also shown as a bold line is a total sum probability curve calculated for each sample from these normal distribution probability curves. This summation of all of the smaller curves does not include the curves with a gray fill color. The latter curves are plots of the normal distribution probability curve for the weighted average ages (with error ranges calculated at the 2 sigma level of confidence) shown on the side of each plot. These weighted average ages were calculated for all the monazite grains separated according to FIA and whether they lie in the core, median or rim of a given garnet porphyroblast, or the matrix as indicated.

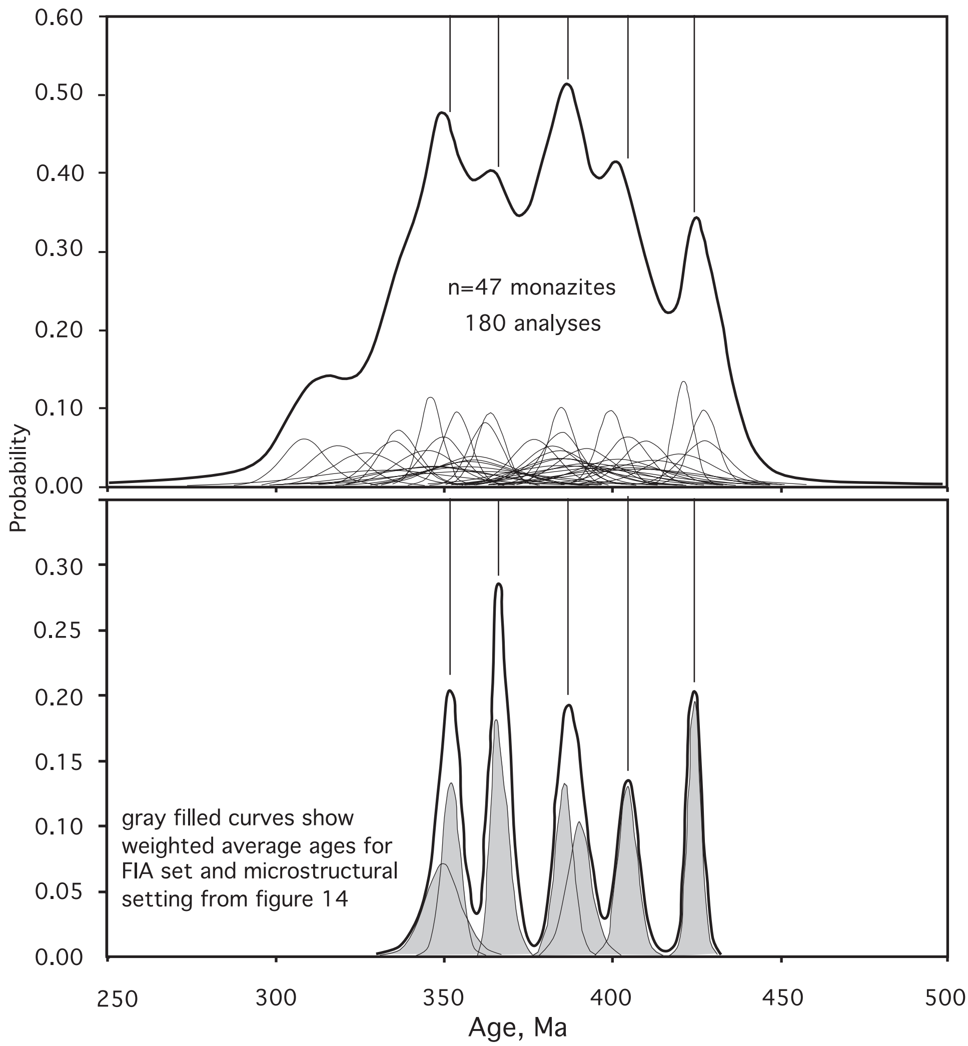

Fig. 15. Probability density curve for all 47 ages of individual monazite grains obtained from the four samples grouped together and using all 180 analyses. This can be compared with the individual sample curves in figure 14 and shows that the ages calculated based on FIA and microstructural setting is reflected in the total distribution.

DISCUSSION

The Heterogeneity of Deformation and FIA Development

Deformation within the earth's crust is inherently heterogeneous due to competency contrasts from the grain scale upwards in rocks (Bell, 1981). This heterogeneity results in partitioning of the deformation into zones of progressive shortening, consisting of low coaxial strain, and zones of progressive shearing consisting of high non-coaxial strain. In contrast, the driving force for orogenesis, the collision between plates, is a very steady state process, with the exception of the effects associated with a change in the direction of relative plate motion. The dates reported herein suggest that deformation and metamorphism during the Acadian extended for at least 80

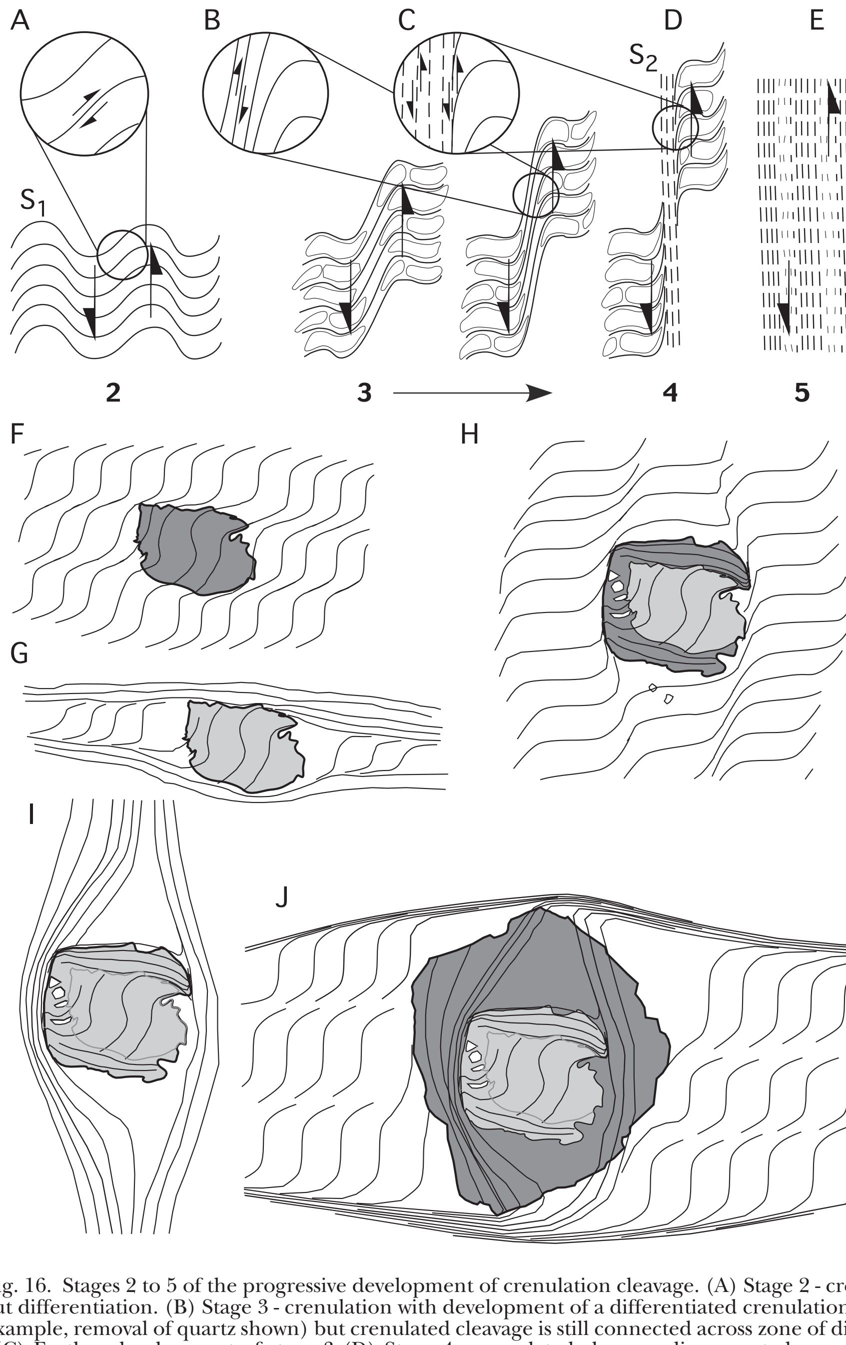

Fig. 16. Stages 2 to 5 of the progressive development of crenulation cleavage. (A) Stage 2 - crenulation without differentiation. (B) Stage 3 - crenulation with development of a differentiated crenulation cleavage (for example, removal of quartz shown) but crenulated cleavage is still connected across zone of differentiation. (C) Further development of stage 3 (D) Stage 4 - crenulated cleavage disconnected across zone of differentiation by shear or recrystallization of new phyllosilicates along the differentiated crenulation cleavage. (E) Stage 5 is destruction of the crenulated cleavage. Stages 1 and 6, which are not shown, are the non-differentiated starting and ultimate foliations. Adapted from Bell (1986). Large arrows indicate bulk shear sense. Small arrows indicate local shear sense between layers/crystals in the matrix. (F) Shows nucleation and growth of porphyroblast prior (dark shading) to development of stage 3 of crenulation cleavage development. (G) Represents development of stage 4 truncational matrix foliation around the porphyroblast. (H) Nucleation of a new stage of porphyroblast growth (dark shading) over portion formed in F, shown in light shading, prior to development of stage 3 of crenulation cleavage development . (I) Development of a truncational matrix cleavage from H to stage 5 or 6. (J) Growth of 3rd stage of porphyroblast growth prior (dark shading) to stage 3 of crenulation cleavage development with preservation of stage 3 in the strain shadow and stage 4 or 5 in the matrix away from the porphyroblast.

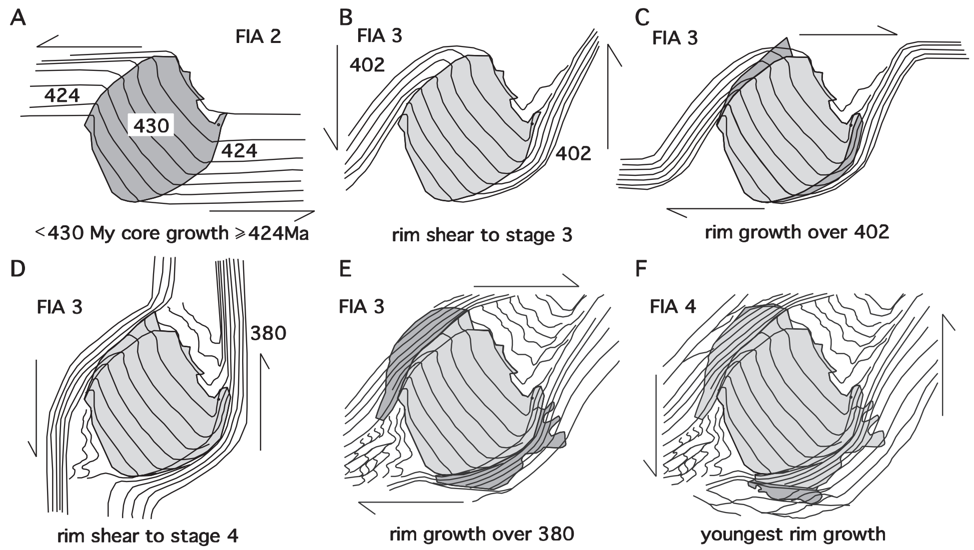

Fig. 17. Sketches showing several stages in the development of the garnet porphyroblast microstructure are shown for sample V634A in figure 5. Dark gray shade indicates portions of porphyroblast that have just grown. Light gray shade indicates portions that grew earlier. The 430 Ma inclusion trails with a preserved Set 1 FIA were crenulated during growth of the garnet that accompanied the development of FIA set 2 as defined by the curvature of the inclusion trails in the core and shown herein (A). The matrix foliation was crenulated to stage 3 of development during the formation of FIA set 3, and resetting monazite ages to 402 Ma (B), before being overgrown by garnet during crenulation by another event as shown in (C). Further deformation during the continued formation of FIA set 3 caused intense shearing and differentiation to stage 4 of crenulation cleavage development against the rim of the porphyroblast at 380 Ma (D). This was overgrown during a younger deformation that also occurred during the development of FIA set 3 (E). The resulting differentiation associated with the horizontal shearing show in E was overgrown by garnet during the development of FIA set 4, which is present in the rim, and resulted in the final geometry shown in (F). This sample contains no evidence for any younger matrix deformation apart from that associated with garnet rim growth during the development of FIA set 4 in F.

million years. The history of deformation and metamorphism recorded by the FIAs is far more extensive than that recorded by the matrix and Bell and others (1998) have shown that some samples contain extensive histories of multiple foliation development around the one FIA trend. This is supported by the extended history of foliation development and monazite ages associated with the development of FIA set 3 in sample V634A that is shown in figure 17. Although structural geologists routinely attempt to correlate matrix foliations from outcrop to outcrop, they have realized that this is fraught with difficulty (Hobbs and others, 1976). The integration of FIA data, detailed microstructural studies of porphyroblasts and geometrical studies of large-scale folds (Bell and Hickey, 1997; Hickey and Bell, 2001) has demonstrated that foliations cannot be correlated from sample to sample within porphyroblasts but FIAs can. However, each FIA develops over a period of time with some samples recording several foliations accompanying FIA development and others only one. Consequently, different foliations defining a particular FIA can have formed at any stage over the period of time that the relative plate motion that developed that FIA trend remained constant. There were nine changes in the relative direction of plate motion between Africa and Europe associated with the development of the European Alps from 115 million years ago to the present day ranging from 31 to 9 million years apart (Platt and others, 1989). So foliation ages associated with the development of a particular FIA could range over similarly varying lengths of time. We have reported detailed dating of monazite grains in four samples. We cannot define the range of ages for each FIA trend at this stage, but should be able to in the years ahead when much more of this type of work has been done within the Appalachians. This should be kept in mind when viewing the total distribution of monazite ages and associated FIA sets in figures 14 and 15. The peaks in this distribution belong to the FIA sets shown but the age boundaries of those FIA sets have not yet been pinned down. Our best estimate so far of the age ranges for the FIA sets 1 through 4 are prior to 425 Ma, from 425 Ma to 400 Ma, from 400 Ma to 375 Ma, and from 375 Ma to 350 Ma. The matrix ranges from 360 Ma to 340 Ma with some evidence for local resetting down to 316 Ma.

Confirmation of the Episodic Nature of Metamorphism

It has been argued for over a decade that the microstructural record of foliation development preserved within porphyroblasts indicates that porphyroblast growth is episodic rather than discrete or continuous (for example, Bell and Johnson, 1989; Bell and Hayward, 1991; Jones, 1994; Williams, 1994; Spiess and Bell, 1996; Adshead-Bell and Bell, 1999). The age data presented herein confirms the episodic nature of porphyroblast growth indicated by the microstructures. Yet garnet porphyroblast growth in these rocks has occurred by a series of continuous reactions that did not go to completion over several phases of porphyroblast growth rather than a discrete set of univariant reactions. That is, some periods of episodic growth of garnet, separated by millions of years, were not the result of changes in the reaction that took place. We believe that an explanation for this phenomenon lies in combining Bell and Hayward's (1991) deformation controls on micro-metasomatic access of the material needed for porphyroblast growth, with the role of strain energy on the activities of the components involved in the reactions (Wintsch and Dunning, 1985). This is currently being investigated further (Bell and Wintsch, unpublished data).

Significance of Episodic Growth of Porphyroblasts

Episodic growth of a porphyroblastic phase without the necessity for a change in the reaction producing that phase, has considerable significance for metamorphic geologists. A reaction is regarded as going to completion once the temperature and pressure for that reaction to proceed has been reached or overstepped (for example, Spear, 1993). Although microstructural indications that this is not the case have been described and discussed for many years, this has had little impact on many metamorphic petrologists because the equilibrium approach suggests that the only control is temperature and pressure (for example, Spear, 1993). Microstructural evidence that porphyroblast growth reactions only occur at the commencement of deformation can possibly be rationalized in terms of the equilibrium approach by suggesting that the reaction slows down by orders of magnitude once stage 3 of crenulation cleavage development (fig. 16B, F, H) has been reached because of diminishing access of the components needed for the reaction to continue (Bell and Hayward, 1991). However, we have never been able to demonstrate that porphyroblast growth continues in a single deformation event once stage 2 of crenulation cleavage development (fig. 16A) for that event has been passed. This is strongly supported by the succession of ages of monazite grains from the core to rim of porphyroblasts in sample V634A (figs. 5 and 6; for example, Adshead-Bell and Bell, 1999; Bell and Hickey, 1999; Hickey and Bell, 1999).

The Age of the Acadian

Figure 14 and table 2 show that the forty-seven individual monazite grains within the four samples dated range in age from 432 to 309 Ma. We set out to date a previously determined FIA succession (Bell and others, 1998) using monazite grains preserved within the foliations that define the FIAs. If these rocks had been dated without this FIA data, this range probably would have been interpreted as reflecting one period of

Acadian metamorphism around 370 Ma in spite of the precision of the ages of individual monazite grains toward either end of the age range. However, the consistent FIA succession and matching progression of dates reveal that this spread of ages is due to episodic but, overall, essentially continuous deformation and metamorphism from at least the 425 to 340 Ma suggested by the peaks on the probability distribution for all samples (fig. 15). The progression of FIAs is directly reflected by a succession in ages. The relationship is so strong that this FIA succession could potentially be used to correlate ages along the orogen.

Acadian Versus Taconic Orogenesis

The oldest age around 425 Ma obtained in this study (fig. 14A) was derived from an early foliation in the cores of garnet porphyroblasts preserving the oldest FIA (sample V634A). Approximately 60 kilometers to the north north east of the Chester Dome, along the same regional anticlinorium axis, lies the Pomfret Dome. The rocks surrounding this dome contain the same succession of FIA trends as those in the region around the Chester and Athens domes, except for an earlier formed NW-SE trending FIA set (Bell and others, 1998; Ham, ms, 2001). We suggest that deformation and metamorphism began in the rocks around the Pomfret dome prior to 425 Ma but did not affect the region around the Chester and Athens domes, or alternatively, no porphyroblasts grew at that time in the latter region to preserve the older ages. In recent years the age for the Taconic orogeny has been extended well into the Ordovician (Ratcliffe and others, 1998). It may eventuate that the break between them, suggested by previous workers, did not occur within the core of the orogen and that orogenesis was essentially continuous from the Taconic through the Acadian to less than 350 Ma.

Continuity of Plate Motion Versus Few Matrix Deformation Events

The small number of deformation events preserved within the matrix of rocks that have undergone orogenesis versus the continuous nature of relative plate motion, led to the suggestion that individual deformation events result from successive collision of continents or island arcs carried by the plate undergoing subduction (for example, Kent and Keppie, 1988). However, the data presented herein, and FIA data in general, suggests deformation is episodic but overall continuous throughout the whole period that plates are colliding, independent of whether an island arc or continent, carried in on the plate being subducted, collides with the subduction zone. The successions of sub-vertical and sub-horizontal foliations that are trapped in porphyroblasts, and that cause the different trending successions of FIAs to form, cannot be readily explained in any other way. The limited number of deformations preserved in the matrix of orogenic belts results from reactivation of earlier formed foliations and decrenulation of newly forming crenulation cleavages (Bell, 1986).

ACKNOWLEDGMENTS

Bell acknowledges the Australian Research Council for funding the research. We both acknowledge Kevin Blake and access to the monazite dating facilities established at the University of Massachusetts where we did the analyses and Mike Williams for all his help in that regard. We gratefully acknowledge the efforts of Boswell Wing and an anonymous reviewer whose detailed reviews enabled us to dramatically improve the manuscript.

References

Adshead-Bell, N.S., and Bell, T.H., 1999, The progressive development of a macroscopic upright fold pair during five near-orthogonal foliation-producing events: complex microstructures versus a simple macrostructure: Tectonophysics, v. 306, p. 121-147.

Armstrong, T.R., Tracy, R.J., and Hames, W.E., 1992, Contrasting styles of Taconian, Eastern Acadian and Western Acadian metamorphism, central and western New England: Journal of Metamorphic Geology, v. 10, p. 415-426.
Bell, T.H., 1981, Foliation development - the contribution, geometry and significance of progressive, bulk, inhomogeneous shortening: Tectonophysics, v. 75, p. 273-296.
Bell, T.H., 1986, Foliation development and refraction in metamorphic rocks: reactivation of earlier foliations and decrenulation due to shifting patterns of deformation partitioning: Journal of Metamorphic Geology, v. 4, p. 421-444.
Bell, T.H., and Cuff, C., 1989, Dissolution, solution transfer, diffusion versus fluid flow and volume loss during deformation/metamorphism: Journal of Metamorphic Geology, v. 7, p. 425-448.
Bell, T.H., and Hayward, N., 1991, Episodic metamorphic reactions during orogenesis: The control of deformation partitioning on reaction sites and duration: Journal of Metamorphic Geology, v. 9, p. 619-640.
Bell, T.H., and Hickey, K.A., 1997, Distribution of pre-folding linear indicators of movement direction around the Spring Hill synform, Vermont: significance for mechanism of folding in this portion of the Appalachians: Tectonophysics, v. 274, p. 275-294.
——— 1999, Complex microstructures preserved in rocks with a simple matrix: significance for deformation and metamorphic processes: Journal of Metamorphic Geology, v. 17, p. 521-536.
Bell, T.H., and Johnson, S.E., 1989, Porphyroblast inclusion trails: The key to orogenesis: Journal of Metamorphic Geology, v. 7, p. 279-310.
Bell, T.H., Fleming, P.D., and Rubenach, M.J., 1986, Porphyroblast nucleation, growth and dissolution in regional metamorphic rocks as a function of deformation partitioning during foliation development: Journal of Metamorphic Geology, v. 4, p. 37-67.
Bell, T.H., Johnson, S.E., Davis, B., Forde, A., Hayward, N., and Wilkins, C., 1992, Porphyroblast inclusion-trail orientation data: eppure non son girate!: Journal of Metamorphic Geology, v. 10, p. 295-307.
Bell, T.H., Forde, A., and Wang, J., 1995, A new indicator of movement direction during orogenesis: measurement technique and application to the Alps: Terra Nova, v. 7, p. 500-508.
Bell, T.H., Hickey, K.A., and Upton, G.J.G., 1998, Distinguishing and correlating multiple phases of metamorphism across a multiply deformed region using the axes of spiral, staircase and sigmoidal inclusion trails in garnet: Journal of Metamorphic Geology, v. 16, p. 767-794.
Bradley, D.C., 1983, Tectonics of the Acadian Orogeny in New England and adjacent Canada: Journal of Geology, v. 91, p. 381-400.
Doll, C.G., Cady, W.M., Thompson, J.B., Jr., and Billings, M.P., 1961, Centennial geologic map of Vermont: Vermont Geological Survey, scale 1:250000.
Ern, E.H., Jr., 1963, Bedrock geology of the Randolph Quadrangle, Vermont: Vermont Geological Survey Bulletin, v. 21, 96 p.
Ham, A.P., ms, 2001, The integration of porphyroblast growth with the microstructural and thermal histories during fold development, in the Acadian orogeny of the Vermont Appalachians: Ph.D. thesis, James Cook University, Townsville, 278 p.
Harrison, T.M., Grove, M., McKeegan, K.D., Coath, C.D., Lovera, O.M., and Le Fort, P., 1999, Origin and episodic emplacement of the Manaslu intrusive complex, central Himalaya: Journal of Petrology, v. 40, p. 3-19.
Hayward, N., ms, 1991, Orogenic processes, deformation and mineralization history of portions of the Appalachian orogen, USA, based on microstructural analysis. Ph.D. thesis, James Cook University, Townsville, 302 p.
Hayward, N., 1992, Microstructural analysis of the classic snowball garnets of southeast Vermont: Evidence for non-rotation: Journal of Metamorphic Geology, v. 10, p. 567-587.
Hepburn, J.C., Trask N. J., Rosenfeld, J.L., and Thompson, J.B., Jr., 1984, Bedrock Geology of the Brattleboro Quadrangle, Vermont-New Hampshire: Vermont Geological Survey Bulletin, v. 32, 192 p.
Hickey, K.A., and Bell, T.H., 1999, Behaviour of rigid objects during deformation and metamorphism: a test using schists from the Bolton Synform, Connecticut: Journal of Metamorphic Geology, v. 17, p. 211-228.
——— 2001, Resolving complexities associated with the timing of macroscopic folds in multiply deformed terrains The Spring Hill synform, Vermont: Bulletin of the Geological Society of America, v. 113, p. 1282-1298.
Hobbs, B.E., Means, W.D., and Williams, P.F., 1976, An outline of structural geology: New York, McGraw Hill, 571 p.
Jones, K.A., 1994, Progressive metamorphism in a crustal-scale shear zone: an example from the Leon region, north-west Brittany, France: Journal of Metamorphic Geology, v. 12, p. 69-88.
Kent, D.V., and Keppie, J.D., 1988, Silurian-Permian palaeocontinental reconstructions and circum-Atlantic tectonics, *in* Harris, A.L., and Fettes, D.J., editors, The Caledonian-Appalachian Orogen: Geological Society Special Publication 38, p. 469-480.
Lanzirotti, A., and Hanson, G.N., 1996, Geochronology and geochemistry of multiple generations of monazite from the Wepawaug Schist, Connecticut, USA; implications for monazite stability in metamorphic rocks: Contributions to Mineralogy and Petrology, v. 125, p. 332-334.
Mancktelow, N.S., 1981, Strain variation between quartz grains of different crystallographic orientation in a naturally deformed metasiltstone: Tectonophysics, v. 78, p. 73-84.
Moecher, D. P., 1999, The distribution, style and intensity of Alleghanian metamorphism in south-central New England: Petrologic evidence from the Pelham and Willimantic Domes: Journal of Geology, v. 107, p. 449-471.
Montel, J.M., Foret, S., Veschambre, M., Nichollet, C.H., and Provost, A., 1996, Electron microprobe dating of monazite: Chemical Geology, v. 131, p. 37-53.

Montel, J.M., Kornprobst, J., and Vieleuf, D., 2000, Preservation of old U-Th-Pb ages in shielded monazite: an example from the Beni Bousera Hercynian kinzigites (Monocco): Journal of Metamorphic Geology, v. 18, p. 335-342.
Page, R.W., and Bell, T.H., 1986, Isotopic and structural responses of granite to successive deformation and metamorphism: Journal of Geology, v. 94, p. 365-379.
Parrish, R.R., 1990, U-Pb dating of monazite and its application to geological problems: Canadian Journal of Earth Science, v. 27, p. 1431-1450.
Platt, J.P., Behrmann, J.H., Cunningham, P.C., Dewey, J.F., Helman, M., Parish, M., Shepley, M.G., Wallis, S., and Weston, P.J., 1989, Kinematics of the Alpine arc and the motion history of Adria: Nature, v. 337, p. 158-161.
Ratcliffe, N.M., 1993, Bedrock geologic map of the Mount Snow and Readsboro Quadrangles, Bennington and Windham counties, Vermont: United States Geological Survey Miscellaneous Investigation Series Map I-2307, scale 1:24000.
——— 1995a, Digital bedrock geologic map of the Cavendish Quadrangle, Vermont: United States Geological Survey Open-File Report 95-203-A.
——— 1995b, Digital bedrock geologic map of the Chester Quadrangle, Vermont: United States Geological Survey Open-File Report 95-576-A.
Ratcliffe, N.M., and Armstrong, T.R., 1995, Preliminary bedrock geologic map of the Saxtons River 7.5°x15° Quadrangle, Windham and Windsor Counties, Vermont: United States Geological Survey Open-File Report 95-482.
——— 1996, Digital bedrock geologic map of the Saxtons River 7.5°x15° Quadrangle, Windham and Windsor Counties, Vermont: United States Geological Survey Open-File Report 96-52-A.
Ratcliffe, N.M., Armstrong, T.R., and Tracy R.J., 1992, Tectonic-cover basement relations and metamorphic conditions of formation of the Sadawaga, Rayponda and Athens Domes, southern Vermont, *in* Robinson, P., and Brady, J.B., editors, Guidebook for field trips in the Connecticut Valley region of Massachusetts and adjacent states: New England Intercollegiate Geological Conference, v. 2, p. 257-290.
Ratcliffe, N.M., Hames, W.E., and Stanley, R.S., 1998, Interpretation of ages of arc magmatism, metamorphism, and collisional tectonism in the Taconian orogen western New England: American Journal of Science, v. 298, p. 791.
Rosenfeld, J.L., 1968, Garnet rotations due to the major Paleozoic deformations in southeast Vermont: in Zen, E-an, editor, Studies of Appalachian Geology: New York, Wiley Interscience, p. 185-202.
——— 1970, Rotated garnets in metamorphic rocks: Geological Society of America Special Paper, v. 129, p. 1-105.
Shaw, C.A., Karlstrom, K.E., Williams, M.L., Jercinovic, M.J., and McCoy, A.M., 2001, Electron Microprobe Monazite Dating of ca. 1.7-1.63 and ca. 1.45-1.38 Ga deformation in the Homestake shear zone, Colorado: Origin and early evolution of a persistent intracontinental tectonic zone: Geology, v. 29, p.739-742.
Smith, H.A., and Barreiro, B., 1990, Monazite U-Pb dating of staurolite grade metamorphism in pelitic schists: Contributions to Mineralogy and Petrology, v. 105, p. 602-615.
Smith, H.A., and Giletti, B.J., 1997, Lead diffusion in monazite. Geochimica et Cosmichimac Acta, v. 61, p. 1047-1055.
Spear, F.A., 1993, Metamorphic phase equilibria and Pressure-Temperature-time paths: Mineraological Society of America, Monograph Series, 799 p.
Spear, F.S., and Harrison, T.M., 1989, Geochronologic studies in central New England I: Evidence for pre-Acadian metamorphism in eastern Vermont: Geology, v. 17, p. 181-184.
Spiess, R., and Bell, T.H., 1996, Microstructural controls on sites of metamorphic reaction: a case study of the inter-relationship between deformation and metamorphism: European Journal of Mineralogy, v. 8, p. 165-186.
Stanley, R.S., and Ratcliffe, N.M., 1985, Tectonic synthesis of the Taconic orogeny in Western New England: Bulletin of the Geological Society of America, v. 96, p. 1227-1250.
Thompson, A.B., Tracy. R.J., Lyttle, P., and Thompson, J.B., Jr, 1977, Prograde reaction histories deduced from compositional zonation and mineral inclusions in garnet from the Gassetts schist, Vermont: American Journal of Science, v. 277, p. 1152-1167.
Thompson, J.B., Jr, 1957, The graphical analysis of mineral assemblages in pelitic schists: American Mineralogist, v. 42, p. 842-858.
Thompson, J.B., Jr, and Thompson, A.B., 1976, A model system for mineral facies in pelitic schists: Contributions to Mineralogy and Petrology, v. 58, p. 243-277.
Thompson, J.B., Jr., McLelland, J.M., and Rankin, D.W., 1990, Simplified geologic map of the Glens Falls 1°x2° Quadrangle, New York, Vermont and New Hampshire: United States Geological Survey Miscellaneous Field Studies Map, MF-2073, scale 1:250000.
Vance, D., and Holland, T., 1993, A detailed isotopic and petrological study of a single garnet from the Gassetts Schist, Vermont: Contributions to Mineralogy and Petrology, v. 114, p. 101-118.
Williams, M.L., 1994, Sigmoidal inclusion trails, punctuated fabric development, and interactions between metamorphism and deformation: Journal of Metamorphic Geology, v. 12, p. 1-21.
Williams, M.L., and Jercinovic, M.J., 2002, Microprobe monazite geochronology: putting absolute time into microstructural analysis: Journal of Structural Geology, v. 24, p. 1013-1028.
Williams, M.L., Jercinovic, M.J., and Terry, M.P., 1999, Age mapping and chemical dating of monazite using the electron microprobe: Deconvoluting multistage tectonic histories: Geology, v. 27, p. 1023-1026.
Williams, M.L., Scheltema, K., and Jercinovic, M.J., 2001, High-Resolution Compositional Mapping of Matrix Phases: Implications for Mass Transfer during Crenulation Cleavage Development in the Moretown Formation, Western Massachusetts: Journal of Structural Geology, v.23, p.923-939.
Winstch, R.P., and Dunning, J., 1985, The effect of dislocation density on the aqueous solubility of quartz and some geologic implications: a theoretical approach: Journal of Geophysical Research, v. 90, p. 3649-3653.